THE ASTROPHYSICAL JOURNAL, 380:495–510, 1991 October 20

THE DIFFUSE SOFT X-RAY BACKGROUND AS SEEN WITH THE *EINSTEIN OBSERVATORY*

G. MICELA,[1] F. R. HARNDEN, JR,[2] R. ROSNER,[3] S. SCIORTINO,[1] AND G. S. VAIANA[1]
Received 1990 December 10; accepted 1991 May 1

ABSTRACT

We present a systematic survey of the diffuse soft X-ray background as seen directly with the *Einstein Observatory*. Using 1633 selected 1° × 1° fields of view obtained by the Imaging Proportional Counter (IPC) to provide ≈5% sky coverage, with some bias toward the Galactic plane, we are able to spatially resolve the background in the 0.16–3.5 keV spectral region on this angular scale. The moderate energy resolution of the IPC also enables us to characterize and produce maps of the background at different energies within the *Einstein* passband. We confirm that the Galactic ridge is not present at energies below 0.33 keV and demonstrate that the appearance of the ridge above this energy is not due to hard Galactic sources with a flux above 10^{-13} ergs cm^{-2} s^{-1}. We have identified a southern Galactic region, with l between 80° and 180° and b less than −5°, where the mean background intensity has the lowest value and is homogeneous within better than 9%; the background in this region likely represents an isotropic component with mean intensity, in the (9.16–2.7 keV energy range) of ≈19 keV cm^{-2} keV^{-1} sr^{-1}, ∼2.5 times more than the value extrapolated from higher energy measurements. We discuss the implications of our results for Galactic structure and for the nature of the extragalactic X-ray background.

Subject heading: X-rays: sources

1. INTRODUCTION

The nature and origin of the "diffuse" soft X-ray background has been a subject of intense interest since the beginnings of X-ray astronomy (Giacconi et al. 1962). Largely as a result of a succession of rocket flights by groups from Wisconsin and Japan, as well as a succession of US and European satellite experiments, a fairly complete picture of the background emerged by the end of the 1970s (cf. Schwartz 1978; Kraushaar 1979; Boldt et al. 1979; McCammon et al. 1983; McCammon & Sanders 1990 and reference therein). On an angular scale of roughly 6° × 6°, the background was distinctly different in character as one went from photon energies of less or equal than 0.1 keV to photon energies of 1 keV and more: at the lower energies, there was considerable evidence of dominance by a diffuse large angular scale, local (e.g., Galactic) emission component, whereas as one increased the photon energy, contributions from extragalactic components became more and more pronounced. Furthermore, it was clear that a prominent Galactic feature, namely the so-called Galactic ridge (cf. Worrall et al. 1982; Koyama et al 1986b), was present, even at energies of a few keV. This structure is one of a host of Galactic features which are superposed on a relatively smooth (on a 6° angular scale) Galactic component, and which have also been seen at lower energies, just below the carbon edge; the most prominent of these was undoubtably identified with the North Polar Spur (Borken & Iwan 1977; Hayakawa et al. 1979; cf. also McCammon et al. 1983 and references therein), a feature first recognized at radio wavelengths, and suggested to be a supernova remnant (cf. Spoelstra 1972; Berkhuijsen 1973).

The obvious question is what the origins of these emissions are. The principal candidates for the Galactic component are the various types of discrete X-ray sources (such as normal stars and binary X-ray sources) and diffuse gas (possibly associated with supernova remnants); for the extragalactic component, the principal candidates are quasars, Seyfert galaxies and other active galaxies, diffuse gas associated with halos of galaxies and clusters of galaxies, and finally diffuse intercluster gas. It was realized early on that the best method to identify the background contributors is to look at the background with high angular resolution, especially if one can also obtain spectral information. Indeed, if one also has sufficient sensitivity, one might even be able to resolve directly the discrete contributors. These concerns in fact directly motivated the so-called Deep Surveys (Giacconi et al. 1979b; Griffiths et al. 1983; Primini et al. 1991), based on the longest exposures made with the *Einstein Observatory* (Giacconi et al. 1979a).

With these concerns in mind, we have focused on a new type of analysis, based on looking directly at the background itself in 1633 *Einstein* Imaging Proportional Counter (IPC; Gorenstein, Harnden, & Fabricant 1981) pointings. By using each one of these pointings as a 1° × 1° sample window on the diffuse soft X-ray background, we have been able to obtain a new look at the soft component of the diffuse background on a relatively fine angular scale (at least when compared to the previous rocket, *Ariel V*, *HEAO 1*, *OSO 8*, and *Tenma* surveys). Our study is complementary to the recent finer angular-scale studies reported by Hamilton & Helfand (1987) and by Barcons & Fabian (1989), which deal only with the much smaller subset of available points used for the *Einstein* Deep Surveys and LMC surveys; preliminary results of our study have been presented elsewhere (Micela et al. 1989a, b, 1990).

A key aspect of the work reported here is the demonstration that an astrophysically meaningful background signal can be extracted from the 1° × 1° IPC fields. Separating this signal from the particle and instrumental backgrounds known to exist in the IPC has enabled us to map diffuse soft X-ray emission using a substantial subset of the full set of exposures taken with the *Einstein* IPC and to determine the spectrum of the large-scale Galactic structures and of the isotropic com-

[1] Osservatorio Astronomico di Palermo Piazza del Parlamento 1 (Palazzo dei Normanni) 90134 Palermo, Italy.
[2] Harvard-Smithsonian Center for Astrophysics, 60 Garden Street, Cambridge, MA 02138.
[3] Department of Astronomy and Astrophysics and Enrico Fermi Institute, The University of Chicago, 5640 South Ellis Avenue, Chicago, IL 60637.

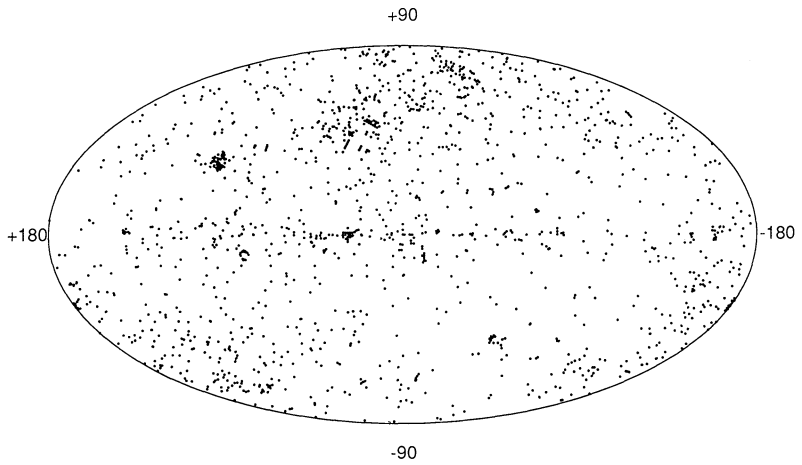

FIG. 1.—Summary plot of the *Einstein Observatory* pointings to which this paper is restricted, which eliminated from the full sample of all pointings all fields with large numbers of point sources, discrete diffuse emission (such as that associated with known supernova remnants, Galactic and cluster halos, etc.), and very short exposure times. The resulting restricted sample contains some 1633 fields, or roughly 5% coverage of the sky.

ponent in the (0.16–3.5 keV) energy band. The fact that this separation can in fact be done bodes well for similar work to be carried out with the X-ray imaging experiments following *Einstein*, such as *ROSAT*, *AXAF*, and *XMM*.

In the next section, we detail the analysis procedures employed in carrying out this survey. Our principal results for the spatial structure of the background are presented in § 3, and a presentation of the spectral results is given in §§ 4 and 5. A summary and discussion is found in the last section (§ 6). Some of the more technical details regarding the analysis procedures are found in the Appendices.

2. METHOD OF ANALYSIS

The IPC obtained 3996 pointings during the course of the *Einstein* mission. Sensitive to X-rays in the energy range of ~0.2–4.0 keV, this imaging detector was used primarily to study discrete sources ranging from ordinary stars to supernova remnants, binary X-ray sources, galaxies, AGNs, and quasars. Since extended sources such as supernova remnants and Galactic and Galaxy cluster halos constituted only a small fraction of the IPC targets, and since only a few discrete point sources appear in the typical IPC field (Harnden et al. 1990), for most IPC fields a large portion of the sensitive area can be used to study diffuse background emission. However, the detector also was sensitive to a combination of detector noise, particle background, and intermittent contamination due to fluorescence of Earth's outer atmosphere in response to incident solar X-rays. The rather involved process of extracting the cosmic diffuse background contribution from these various contaminating components[4] was considerably eased by features implemented in the REV-1B analysis (Harnden et al. 1984) of the complete set of IPC fields installed in the form of an Ingres[tm] data base (Sciortino et al. 1988; Harnden et al. 1990).

From an initial set of 3996 IPC fields (Harnden et al 1990) we eliminated all fields with obvious difficulties: (*a*) 1964 fields containing large amounts of solar-fluorescent emission from Earth's atmosphere, (*b*) 46 fields with exposure times below 5×10^2 s (omitted in order to avoid difficulties with low signal-to-noise ratio background data), and (*c*) 353 fields with extended and/or strong point sources (for more details, see Appendix A). The remaining 1633 "cleaned" fields formed the basis for the analysis discussed below; a total of approximately 8.2×10^5 counts were contained in these annuli.

The Galactic distribution of these pointings is shown in Figure 1, and Table 1 provides the full list of sequence numbers used in this work. For these fields, we then used the annular background determination provided by the ReV-1B processing (Harnden et al. 1984) to determine the background count rate in each field in the nominal 0.16–3.5 keV bandpass. Considerable care was needed, as described in Appendix A, to ensure that all noncosmic contributions were excluded from the final annular background rates.[5]

Figure 2 shows the actual frequency distribution of the background rates (*solid line*) determined from our analysis of all IPC fields in the "cleaned" set of points (cf. Appendix A), and the corresponding *expected* distribution (*dashed line*) obtained from a Monte Carlo simulation which took the observed median background rate as the best estimate of "true" rate, and assumed Poisson counting statistics to synthesize the distribution. It is clear even on cursory inspection that the observed distribution is significantly wider than the simulated one; a two-sample Kolmogorov-Smirnov test confirms this conclusion at a confidence level greater than 99.9999%. Since we cannot account for the spread in the observed distribution as statistical or instrumental detector effects (cf. discussion in the next section and in Appendix B), we therefore argue that the distribution must reflect the nature of the actual cosmic background. Note that the results shown in Figure 2 do not allow one to deduce the spatial scales of the "signal" which

[4] Note that not all of these "contaminants" are really astrophysically irrelevant; for example, Schmitt, Fink, & Harnden (1987) showed recently that by looking at the diffuse fluorescent emission from Earth's atmosphere, it is possible for *Einstein* to follow a solar flare—and as a result to demonstrate explicitly for the first time that stellar X-ray flares are indeed remarkably similar to their solar counterparts.

[5] Although somewhat better statistics could be obtained by using the entire IPC field of view, rather than just the background annulus, the combined effects of vignetting and (substantial) systematic uncertainties in detector parameters at off-axis angles beyond the annulus render the results of such an extension of the analysis more uncertain.

TABLE 1

Einstein Observatory IPC Fields Used in This Work

129	490	871	1960	2241	2701	3200	3513	3936	4235	4603	5116	5549	6208	6820	7356	7776	8459	9156
130	491	873	1961	2243	2702	3204	3515	3942	4239	4605	5118	5562	6218	6841	7359	7786	8460	9163
131	492	885	1967	2244	2705	3210	3516	3943	4241	4606	5121	5564	6220	6842	7360	7790	8461	9183
133	494	889	1970	2246	2710	3212	3517	3946	4242	4607	5126	5565	6253	6844	7362	7791	8462	9204
134	495	891	1979	2248	2712	3215	3518	3948	4244	4610	5143	5567	6271	6847	7364	7793	8468	9225
135	496	893	1982	2250	2713	3216	3520	3964	4247	4611	5147	5576	6311	6854	7391	7795	8490	9257
136	497	895	1983	2251	2807	3217	3521	3965	4248	4613	5148	5578	6315	6881	7404	7796	8570	9258
137	498	905	1985	2253	2823	3239	3522	3967	4249	4614	5150	5581	6328	6888	7405	7798	8590	9283
141	501	915	1987	2259	2828	3242	3523	3969	4250	4615	5152	5584	6339	6898	7406	7802	8593	9285
142	502	916	1989	2261	2911	3247	3524	3970	4251	4616	5157	5599	6348	6907	7410	7803	8645	9469
145	504	917	1991	2269	2949	3254	3526	3972	4253	4619	5159	5602	6361	6918	7413	7805	8652	9470
147	513	919	1995	2273	2952	3255	3527	3973	4254	4620	5174	5605	6369	6926	7414	7812	8653	9471
148	518	1091	1997	2274	3007	3256	3528	3977	4256	4624	5179	5636	6385	6927	7424	7814	8656	9472
154	519	1092	1998	2275	3023	3257	3529	3978	4258	4887	5185	5646	6402	6928	7427	7815	8662	9528
161	524	1099	2011	2277	3025	3261	3530	3979	4260	4889	5190	5660	6407	6929	7431	7818	8664	9542
164	525	1122	2013	2281	3026	3262	3532	3986	4261	4891	5191	5661	6413	6934	7433	7819	8665	9550
165	529	1131	2014	2283	3027	3263	3536	3987	4263	4892	5193	5666	6417	6952	7434	7823	8666	9551
171	532	1142	2015	2291	3032	3264	3549	3988	4264	4893	5205	5669	6419	6976	7440	7828	8670	9552
173	538	1143	2017	2294	3033	3267	3551	3989	4265	4896	5213	5691	6420	6977	7445	7830	8686	9610
182	540	1167	2018	2295	3037	3269	3553	3991	4268	4897	5215	5694	6421	6982	7451	7831	8687	9611
187	543	1168	2031	2297	3038	3275	3555	3992	4293	4901	5220	5698	6428	6984	7462	7834	8688	9612
189	548	1170	2035	2300	3039	3276	3556	3994	4300	4910	5223	5699	6429	6988	7464	7835	8691	9613
190	549	1186	2046	2308	3040	3278	3563	3995	4301	4919	5228	5705	6438	6990	7468	7836	8693	9680
191	553	1197	2050	2312	3045	3281	3564	3997	4302	4920	5247	5708	6439	6992	7471	7838	8694	9696
203	565	1198	2051	2332	3050	3284	3582	3999	4306	4921	5248	5717	6442	6993	7473	7841	8696	9704
205	573	1228	2052	2334	3051	3285	3583	4001	4309	4922	5250	5720	6443	6999	7478	7846	8704	9916
206	588	1230	2054	2340	3052	3286	3585	4002	4313	4924	5254	5721	6444	7001	7480	7861	8735	9937
208	591	1233	2055	2346	3053	3292	3586	4003	4314	4925	5255	5726	6449	7011	7482	7864	8736	9941
209	598	1235	2056	2353	3054	3293	3594	4004	4315	4927	5256	5727	6451	7014	7487	7868	8741	10071
212	602	1237	2057	2360	3056	3294	3597	4008	4317	4929	5258	5734	6463	7018	7488	7876	8745	10074
213	603	1238	2058	2388	3066	3297	3621	4016	4374	4930	5276	5742	6465	7023	7506	7879	8752	10082
215	604	1259	2060	2480	3067	3300	3622	4017	4396	4933	5281	5769	6471	7024	7507	7884	8757	10086
225	607	1273	2063	2486	3070	3302	3623	4020	4402	4939	5282	5776	6472	7025	7508	7885	8758	10107
228	608	1274	2073	2494	3071	3303	3624	4023	4403	4941	5306	5777	6493	7034	7510	7886	8767	10109
229	612	1318	2076	2508	3072	3307	3626	4024	4405	4942	5307	5782	6496	7039	7514	7890	8771	10116
233	613	1319	2077	2515	3073	3308	3627	4025	4406	4946	5309	5790	6497	7040	7517	7891	8774	10119
237	616	1750	2082	2516	3074	3312	3647	4034	4409	4950	5312	5791	6571	7049	7520	7892	8787	10120
239	621	1751	2086	2519	3076	3313	3653	4036	4416	4952	5314	5796	6574	7054	7525	7894	8792	10129
240	698	1752	2089	2520	3077	3314	3713	4037	4417	4954	5320	5797	6575	7116	7530	7895	8793	10137
242	703	1753	2092	2522	3080	3316	3714	4045	4419	4958	5321	5799	6576	7118	7559	7896	8803	10150
251	720	1767	2094	2524	3083	3317	3716	4053	4423	4959	5335	5800	6577	7121	7569	7898	8814	10152
252	751	1795	2098	2535	3086	3319	3717	4055	4433	4961	5336	5899	6579	7123	7579	7903	8815	10153
255	768	1801	2102	2536	3087	3321	3718	4056	4435	4962	5337	5900	6581	7126	7582	7906	8819	10157
257	771	1810	2109	2543	3090	3335	3719	4057	4441	4963	5339	5901	6582	7127	7608	7908	8820	10225
265	773	1812	2113	2552	3091	3336	3722	4058	4444	4964	5343	5904	6583	7129	7609	7909	8822	10226
270	778	1813	2123	2568	3092	3339	3727	4059	4446	4965	5347	5906	6584	7130	7610	7910	8823	10228
280	780	1818	2124	2569	3094	3340	3748	4060	4450	4972	5350	5923	6585	7135	7616	7912	8825	10244
281	784	1819	2126	2572	3108	3341	3749	4061	4451	4973	5361	5938	6587	7149	7629	7914	8831	10254
294	785	1823	2127	2573	3109	3351	3757	4062	4453	4974	5365	5943	6589	7152	7630	7915	8846	10294
314	787	1824	2130	2577	3110	3353	3758	4065	4455	4979	5369	5945	6598	7160	7632	7918	8848	10308
315	788	1825	2133	2600	3111	3354	3762	4069	4476	4980	5374	5952	6643	7162	7640	7922	8852	10310
320	790	1827	2134	2601	3115	3358	3771	4070	4493	4983	5375	5955	6644	7166	7641	7923	8861	10386
323	792	1838	2141	2603	3116	3359	3778	4071	4500	4984	5376	5956	6667	7167	7651	7955	8872	10412
329	793	1840	2143	2604	3118	3360	3779	4072	4502	4985	5377	5976	6675	7169	7663	7957	8876	10434
331	794	1842	2144	2606	3122	3363	3780	4075	4505	4989	5378	5983	6681	7170	7664	7965	8880	10437
336	799	1844	2146	2608	3124	3367	3787	4078	4507	4990	5381	5984	6684	7171	7665	7980	8897	10449
337	801	1847	2150	2612	3125	3391	3811	4080	4508	4991	5382	5986	6685	7172	7667	8022	8904	10456
369	803	1849	2155	2615	3126	3392	3812	4084	4509	4992	5383	5987	6687	7176	7671	8028	8907	10497
371	804	1851	2160	2616	3129	3393	3815	4085	4510	4993	5384	5988	6691	7181	7672	8047	8918	10572
411	805	1852	2163	2617	3131	3394	3817	4093	4511	4995	5387	5991	6694	7182	7677	8332	8936	10573
414	807	1854	2171	2621	3133	3405	3820	4094	4512	5021	5388	5992	6695	7185	7682	8333	8957	10608
416	808	1855	2172	2622	3134	3438	3821	4103	4515	5024	5392	5993	6697	7193	7683	8334	8982	10624
421	809	1856	2174	2630	3136	3440	3828	4104	4516	5034	5393	5995	6703	7206	7687	8349	8992	10766
423	810	1857	2175	2633	3140	3442	3830	4107	4518	5039	5394	5996	6704	7221	7690	8355	8996	10768
425	811	1866	2177	2642	3144	3443	3839	4108	4521	5045	5396	5997	6715	7229	7697	8364	9000	10771
426	812	1872	2181	2644	3145	3444	3840	4109	4523	5047	5405	6004	6717	7254	7698	8365	9002	10775
429	813	1873	2184	2651	3146	3447	3841	4111	4526	5048	5407	6005	6719	7256	7700	8371	9004	10776
430	814	1874	2186	2654	3147	3450	3843	4113	4528	5050	5417	6007	6721	7257	7702	8385	9017	
433	830	1875	2187	2655	3149	3453	3872	4114	4529	5055	5418	6018	6722	7278	7704	8386	9027	
435	833	1880	2188	2656	3150	3454	3886	4115	4531	5056	5419	6021	6728	7284	7706	8390	9030	
443	837	1883	2189	2657	3151	3457	3888	4116	4538	5057	5423	6034	6732	7285	7710	8391	9049	
444	839	1884	2194	2661	3153	3466	3890	4117	4541	5060	5428	6037	6734	7287	7728	8393	9050	
445	840	1900	2195	2665	3156	3472	3892	4119	4542	5068	5430	6039	6735	7288	7735	8400	9051	
452	842	1905	2196	2666	3157	3474	3894	4136	4544	5069	5450	6042	6736	7289	7736	8413	9061	
457	843	1907	2202	2672	3167	3475	3899	4137	4545	5071	5453	6056	6740	7291	7737	8423	9084	
460	844	1915	2218	2674	3173	3476	3900	4138	4548	5073	5455	6059	6744	7295	7741	8427	9094	
462	845	1929	2219	2675	3174	3478	3902	4140	4549	5075	5470	6069	6746	7296	7742	8428	9101	
463	846	1937	2222	2676	3176	3479	3908	4144	4551	5089	5471	6071	6775	7297	7743	8429	9113	
464	847	1938	2224	2679	3177	3481	3910	4145	4557	5090	5482	6076	6778	7299	7744	8432	9114	
467	851	1943	2229	2683	3178	3482	3911	4146	4558	5091	5484	6077	6780	7300	7745	8433	9125	
469	852	1945	2230	2684	3181	3490	3916	4147	4575	5092	5485	6084	6782	7306	7751	8437	9130	
470	853	1948	2231	2686	3185	3500	3917	4148	4578	5097	5490	6085	6791	7307	7759	8438	9133	
471	854	1955	2233	2687	3190	3501	3918	4190	4579	5099	5507	6097	6799	7308	7760	8452	9134	
482	856	1956	2234	2688	3195	3506	3920	4199	4580	5103	5517	6098	6802	7309	7764	8454	9136	
487	857	1957	2236	2692	3197	3508	3922	4230	4582	5104	5527	6118	6809	7311	7769	8455	9138	
488	858	1958	2237	2694	3198	3510	3923	4232	4587	5105	5534	6123	6811	7334	7770	8456	9145	
489	865	1959	2240	2695	3199	3511	3924	4233	4602	5114	5545	6128	6812	7344	7772	8458	9146	

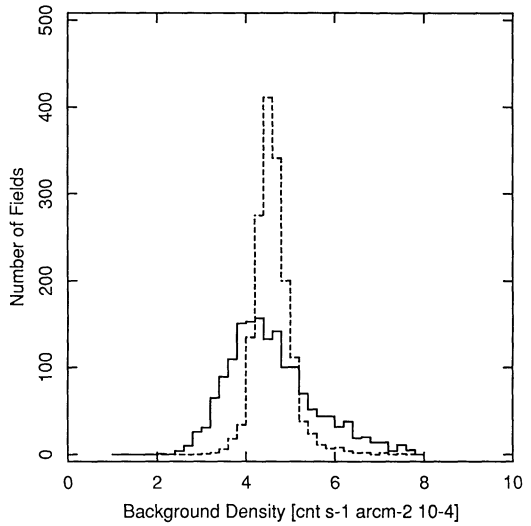

FIG. 2.—The distribution of number of IPC fields of a given background count rate (in counts square arcmin^{-2} s^{-1}) in the actual sample (*solid line*), compared with the results of a Monte Carlo simulation (*dashed line*) which gives the distribution expected under the assumption that the only source of variance in the count rate is the Poisson statistics of the background. This comparison shows conclusively that Poisson statistics in and of itself is incapable of accounting for the observed variance in the mean background count rate.

must be present; the further analysis required to do this is described in the following section.

3. SPATIAL STRUCTURE OF THE DIFFUSE BACKGROUND

A display of the spatial characteristics of the X-ray background, as seen by the IPC, is provided in the false-color intensity map of Figure 3 (Plate 12), which displays the 0.16–3.5 keV sky in Galactic coordinates in the four quartiles of the intensity distribution. Note that the map clearly shows evidence for (*i*) a large emission structure in the northern hemisphere (e.g., the well-known North Polar Spur; cf. Borken & Iwan 1977) and (*ii*) the Galactic ridge (which has been seen earlier in the (2–10 keV) energy range (Worrall et al. 1982) and in the (1.5–11 keV) energy range (Koyama et al. 1986b). We note also that the map (discussed in more detail below) does not show localized regions of enhancement (e.g., the emission associated with large angular size supernova remnants such as Vela; cf. Kahn et al 1985) because of the criteria adopted in field selection (cf. § 2). It is the prominence in our data of these large-scale features, whose presence had been established prior to our studies, which initially encouraged us that the IPC background could yield information on the diffuse, cosmic X-ray background.

3.1. *Spatial Variability*

The analysis we report here covers the sky with an efficiency of roughly 5%; and the data presented in Figure 2, together with the map, shown in Figure 3, bear on the issue of the large-scale structures and granularity of the soft X-ray background. Recall that a crucial aspect of the present analysis is that—because of the imaging capability of the IPC—we are able to remove from the background the effects of all detected point sources, down to a mean point source flux level of $\approx 10^{-13}$ ergs s^{-1} in the 0.16–3.5 keV bandpass. How then are we to explain the observed deviation of the count rate distribution shown in Figure 2 (*solid line*) from a purely random distribution of the type shown in the same figure (*dashed line*)? Recall the well-known fact that if the background were to be entirely due to truly diffuse emission, then its granularity properties would be drastically different than if the background were due to the superposition of emission from point sources which fell below the detection threshold of this survey (cf. Gorenstein & Tucker 1972); hence, the question just posed is intimately tied to the question of what causes the background in the first place.

We performed a classic two-sample Kolmogorov-Smirnov test for the proposition that the observed distribution of the background rate is consistent with a random distribution in each of a set of subregions of the sky shown in Figure 4*a*. As is the case for the entire sample of fields, the results for the individual regions of Figure 4*a* show a deviation of the observed distribution of the background rates from a purely random distribution. In some of these regions, this deviation can be accounted for very simply: these are the regions containing obvious structures in the background, such as the Galactic ridge, and the North Polar Spur. In an effort to understand these deviations from purely random behavior in the fields *not* containing obvious structures, we considered in more detail four distinct factors which contribute to the frequency distribution of the background rate:

1. *Statistical fluctuations* in the actual number of background counts collected in each of the fields we studied; the expected contribution to the variance of the distribution from this component for the full set of fields in our sample has been directly calculated, as remarked above, via Monte Carlo simulations (cf. dashed curve in Fig. 2), and accounts for about the 18% of the total observed variance.

2. *Count rate variations introduced by changes in the ambient particle-background environment* encountered by the spacecraft during the observations. This effect has been extensively studied in the IPC data (Harnden et al. 1984). Appendix B treats this problem in detail and provides a quantitative description of the uncertainty originating from this effect.

3. *Count rate variations due to changes in the susceptibility to solar X-rays scattered from/fluoresced by Earth's outer atmosphere* into the telescope during the observations. We believe the screening procedures described in Appendices A and B have reduced the combined contribution of effects (2) and (3) to no more than 19% of the total variance. Summing up the variances of the various noise contributions to the background, we then estimate that no more than 37% of the total variance, in the observed background rate in the 0.16–3.5 keV energy band, can be due to nonastrophysical effects.

4. *Intrinsic variation of the cosmic diffuse background* on spatial scales larger than 1°. This might occur both because of fluctuations in the number of undetected point sources contributing to distinct IPC fields due to inhomogeneities in the distribution of point sources on angular scales larger than a degree and of inhomogeneities in truly diffuse emission on angular scales larger than a degree.

In our attempts to disentangle the first three effects from the fourth, we examined in further detail the background count rate distributions for each of the regions indicated schematically in Figure 4*a*. The principal divisions are the Galactic equatorial Regions (1 and 2, with 1 enclosing the Galactic center), the high-latitude regions over the central Galactic bulge (Regions 3), and the high-latitude regions toward the Galactic anticenter (Regions 4). We shall repeatedly focus on one specific area of the map, Region 4c, because it contains fields whose background count rate distribution has the lowest

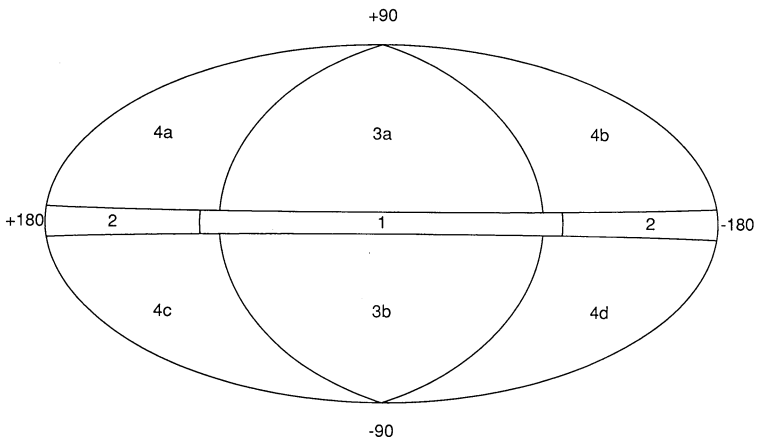

FIG. 4a

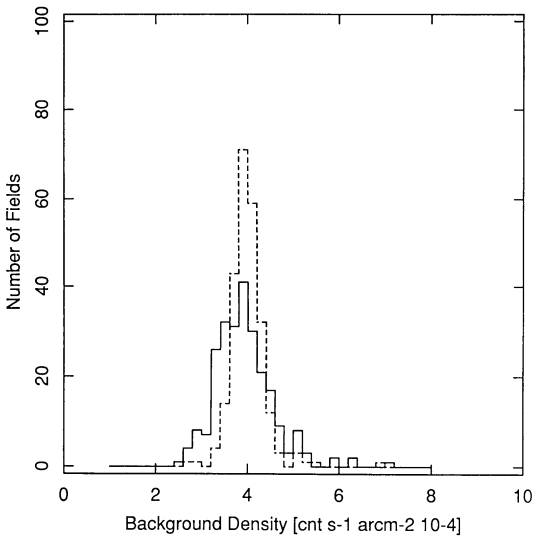

FIG. 4b

FIG. 4.—(*a*) The subdivision of the X-ray sky into distinct regions; note that Region 4c is particularly featureless, as can be seen on inspection of Fig. 3, and hence will be used as the canonical comparison in our discussions. (*b*) The observed count rate distribution in Region 4c (*solid line*), and the expected count rate distribution in Region 4c (*dashed line*), based on Monte Carlo simulations similar to those conducted for Fig. 2. Comparison of these two distribution functions, in addition to a detailed study of the various possible contributors to the IPC background (Appendices A and B), shows that the excess variance in the observed distribution (*b*) is mostly due to non-astrophysical contributions. Since Region 4c X-ray background shows no distinct angular structure, we have, for purposes of this paper, assumed that it is due to the isotropic, largely extragalactic, X-ray background.

mean value and the smallest variance. Since there is no a priori reason for the fields in Region 4c to have particulary low particle or Earth-fluorescence backgrounds, we have assumed as a working hypothesis that it is the actual X-ray background which is lowest there. In order to diminish even further any residual instrumental effects, we have used Region 4c as a reference template and have studied enhancements above its level *differentially* by comparing the background properties of the other regions with those of Region 4c. This procedure leads to the best estimate of the excess background in these other regions.

We have constructed the observed background count rate distribution for Region 4c (shown in Fig. 4*b*, *solid line*), and compared it with a background distribution based purely on count statistics and derived from simulations (shown in Fig. 4*b*, *dashed line*) using the identical distribution median. The observed distribution is significantly wider than the expected one, indicating that above factors (2)–(4) must be contributing significantly to the observed distribution. A comparison of the distribution of Figure 4*b* with those for the full set of fields (Fig. 2), or with distributions constructed for the remaining Regions, shows that the distribution for Region 4c is significantly narrower. This impression is quantified in Figure 5 which presents a quantile-quantile plot[6] (cf. Wilk & Gnanadesikan 1968; Chambers et al 1983; Hoaglin, Mosteller, & Tukey 1985) of the distribution of Region 4c versus that of the "complete" sky and indicates that the distribution have essentially the same shape (up to a value of background density $\approx 6 \times 10^{-4}$ counts^{-1} arcmin^{-2}) but different means (Δ mean ≈ 0.66) and different scales ($\Delta\,\sigma \approx 0.33$). Even if our analysis procedures (cf. Appendices A and B) have left some residual particle and/or fluorescent background uncorrected, there is no reason to expect systematic differences in the noncosmic background contributions for the various fields that make up these different regions; in addition, our estimate of the actual percentage contribution (19%) to the measured variance due to the combined effects of the particle and fluorescent backgrounds falls well below the levels needed to account for the observed distribution in the entire sky. The combined effect of statistical fluctuations, particle and fluorescent backgrounds can explain a large

[6] Quantile-quantile (or "q-q") plots are a useful graphical technique for comparing the shapes of distributions. Suppose, for example, we wish to compare two distributions of some observed variable, with cumulative distribution functions $F(p)$ and $G(p)$, where p is the fraction of the population; we would then vary p over a set of selected values of the observed variable, use the inverse function to obtain $G^{-1}(p)$ and $F^{-1}(p)$, and plot the pairs of data points $[G^{-1}(p), F^{-1}(p)]$. If the two distributions are the same, then these points will lie on a straight line, with slope 1, with its intercept at the origin. If G and F have the same shape but differ in their location or scale, then the intercept and slope, respectively, of this line will change. For example, all Gaussian distributions belong to the same family but can have different mean value (location) and standard deviation (scale). If we compare two Gaussian distributions, one of which we assume to have mean 0 and standard deviation 1, and the other a mean of m and standard deviation σ, we obtain

$$G^{-1}(p) = m + \sigma F^{-1}(p) .$$

In this case, the q-q plot takes the form of a straight line with slope σ and intercept m as long as G and F have the same form; if G and F have different shape, then the q-q plot will of course curve according to the difference in skewness and symmetry of the two distributions.

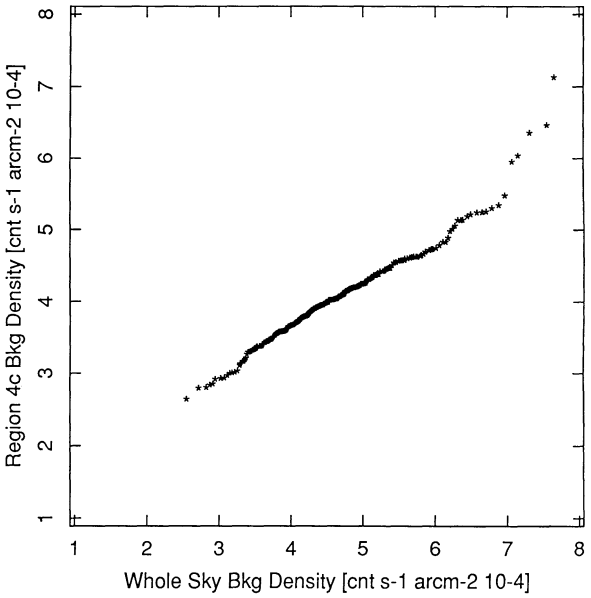

FIG. 5.—Quantile-quantile plot (Chambers et al. 1983) comparison of the 0.16–3.5 keV intensity distributions from the "reference" region, Region 4c, and from the entire data sample; see discussion in text of the significance of the linear shape of this "q-q" plot and its deviation from unity slope and zero intercept.

fraction of the measured variance of background rate in Region 4c.

We are therefore led to the conclusion that the differences in background count rates must be due to real spatial variations in the diffuse X-ray background on spatial scales larger than a degree, a conclusion not in disagreement with the results of Hamilton & Helfand (1987) who have studied the fluctuations of the X-ray background on angular scale of 1′ and of Barcons & Fabian (1989) who have studied the spatial autocorrelation of X-ray background intensity up to 15′ scale (both studies are based on the *Einstein* Deep Survey fields; Giacconi et al 1979b). That is, the distribution of the X-ray background intensity of our data suggests an origin for the background which can produce variation on angular scales of 1° or more. For a better determination of the energy range where these variations occur, we have separately evaluated the variances of background intensity in the IPC Pulse-height Independent (PI; cf. Harnden et al. 1984) channel 2 covering approximately the same energy range of "C-band," and of the summed contributions of PI channels 3, 4, and 5, covering the energy range 0.33–1.08 keV (i.e., approximately the same energy range of "M-band"). The measured variances are 0.245 and 0.077 in the two above bandpasses, respectively. Adopting the same procedure described in § 2, we have estimated that count statistic can explain only 26% and 36% of the measured variances in the two above energy ranges, respectively.

This result contradicts the conventional wisdom that the spatial structure in the so-called "M-band" ($\approx$0.3–1.0 keV, as defined by the Wisconsin sky surveys; cf. McCammon et al. 1983), is basically uniform (aside from localized features of the type mentioned above; cf. Sanders et al. 1983) and casts considerable doubt on this conventional view.

3.2. *Autocorrelation Analysis of Background Fluctuations*

We have attempted a more quantitative characterization of the angular variations in background rate by analyzing the one-dimensional spatial autocorrelation function of the background, based on the angular separation (on the sphere) of all pairs of IPC fields in our background study. This kind of analysis allows us to fix the dominant angular scale (if any) on which the excess background variations seen in Figure 2 occur. Using the procedure of Edelson & Krolik (1988) for constructing discrete correlation functions for unevenly sampled data, we first computed the autocorrelation function and the associated 3 σ error bars (Fig. 6). The comparison of the three autocorrelation functions of Figure 6 shows that in Region 4c (where the mean background intensity is lower) there is no evident (at the 3 σ level) spatial correlation on angular scales up to 70°; this result holds unchanged both in the soft (0.16–0.8 keV) and hard (0.8–3.5 keV) energy bands. The full-sky autocorrelation analysis shows positive correlation on angular scales below $\sim$20°. Correlation on the same angular size range is clearly present in the northern Galactic sky (Regions 4a, 4b, and 3a of Fig. 4*a*), and is most likely due to the presence of the NPS.

The first result (e.g., the lack of measurable correlation of the background in Region 4c on scales of $\approx$3°) has very significant consequences for models of the extragalactic diffuse background. Furthermore, our data and the analysis procedure we have applied allow us to determine the 3 σ upper bound on the amplitude of background fluctuations in the (0.16–3.5) keV energy band. The derived 3 σ upper bounds at $\sim$3° are $\langle \Delta B^2(3^\circ)\rangle^{1/2}/\sigma_{\text{"true"}} \leq 0.64$ (cf. Edelson & Krolik 1988), where $\sigma_{\text{"true"}} = (\sigma_B^2 - \sigma_{\text{stat}_B}^2)^{1/2}$ is the dispersion of the background measurements (σ_B) corrected for the dispersion induced by counting statistic (σ_{stat_B}), or, with an alternative notation (cf. Barcons & Fabian 1989; Persic et al. 1989), $\langle \Delta B^2(3^\circ)\rangle^{1/2}/\langle B\rangle \leq 8.8 \times 10^{-2}$, where $\langle B\rangle$ is the mean background value. The analogous upper bounds in the (0.16–0.8) keV energy band and (0.8–3.5) keV energy band are $\langle \Delta B^2(3^\circ)\rangle^{1/2}/\sigma_{\text{true}} \leq 0.69$, or $\langle \Delta B^2(3^\circ)\rangle^{1/2}/\langle B\rangle \leq 11.1 \times 10^{-2}$, and $\langle \Delta B^2(3^\circ)\rangle^{1/2}/\sigma_{\text{true}} \leq 0.70$, or $\langle \Delta B^2(3^\circ)\rangle^{1/2}/\langle B\rangle \leq 11.0 \times 10^{-2}$, respectively. These values can be used to constrain models for the correlated component of the X-ray background based on discrete extragalactic sources such as AGNs: such models would then require that the class of objects in question have a comparable intrinsic angular correlation. A similar lack of correlation, exploited with *HEAO 1* data, has been recently discussed (cf. Persic et al. 1989; De Zotti et al. 1990). On the basis of our derived upper bounds, sources such as AGNs may well play a central role in accounting for the observed extragalactic background.

3.3. *Discrete Structures*

In addition to the smooth diffuse background just discussed, there are large-scale structures for which substantial previous observations exist. The most prominent, which we discuss in the following, can be used as a test of our procedures, as well as a calibration of the analysis itself.

The Galactic ridge.—It has been known for some time that in addition to the hard isotropic (at the $\approx$3% level) extragalactic component and to the very soft local Galactic background, there is an X-ray background associated spatially with the Galaxy, consisting of two distinct components: the first is rather hard (consistent with a $\approx$9 keV bremsstrahlung spectrum) and has a scale height of several kiloparsec (cf. Iwan et al. 1982); the second is somewhat softer (for thermal bremsstrahlung models, the best-fit temperatures lie in the several keV range and has a substantially smaller scale height of $\approx$240 pc

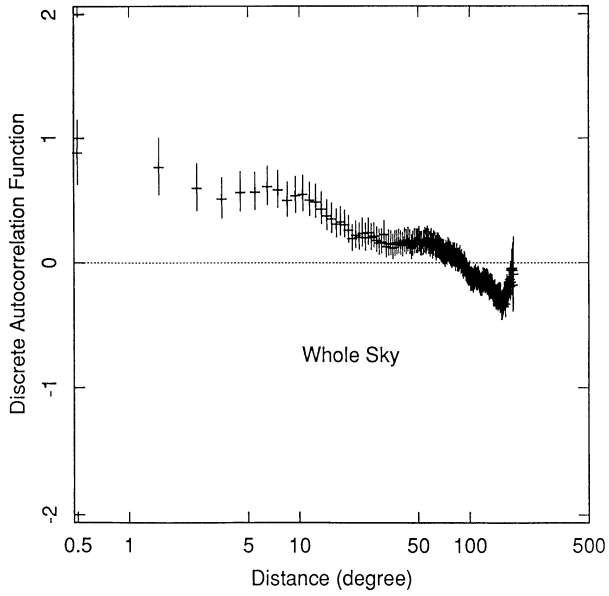

FIG. 6a

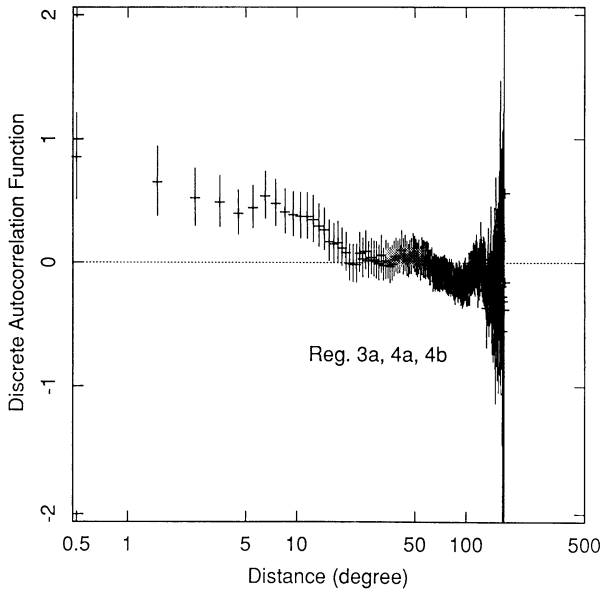

FIG. 6b

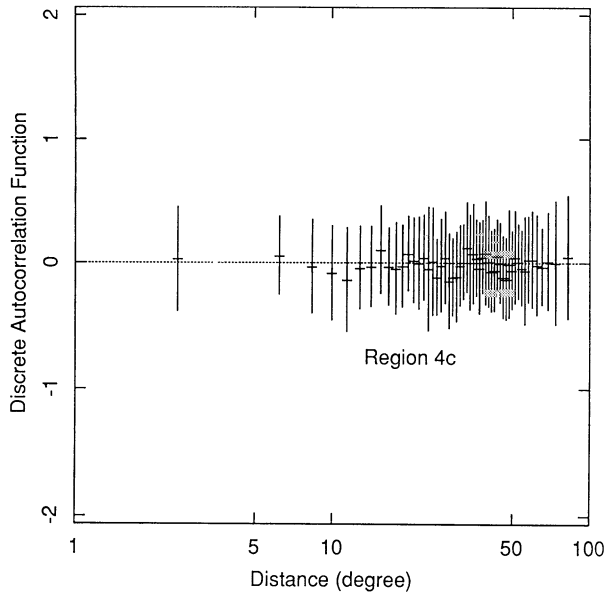

FIG. 6c

FIG. 6.—One-dimensional, spatial discrete autocorrelation functions (cf. Edelson & Krolik 1988) for (*a*) the entire data set, (*b*) the set of data from northern Galactic sky, and (*c*) the data from the "reference" Region 4c. All error bars are shown at the 3 σ level. Note the evidence for lack of any significant spatial correlation on angular scales up to 70°, seen in panel (*c*).

above the Galactic equator (cf. Nousek et al. 1982; Worrall et al. 1982). These two components were observed earlier by *Uhuru* (Protheroe, Wolfendale, & Wdowczyk 1980) and *Ariel* (Warwick, Pye, & Fabian 1980) but were not clearly separated until the *HEAO 1* observations by Iwan et al. and others were carried out. The second background component was actually first seen much earlier by a rocket experiment in the 2–10 keV range (cf. Bleach et al. 1972). In addition the very soft surveys by the Wisconsin group showed definitively that this Galactic plane component extended down into the 0.3–1.0 keV range, but not below roughly 0.3 keV, at least at the angular resolution ($\sim 7°$) of the Wisconsin data (see Nousek et al. 1982; Sanders et al. 1983). Most recently, Koyama (1988a, b) reported that this "Galactic ridge" component has also been seen by *Ginga* in the 2–37 keV energy range. We note that the IPC is the first instrument capable of imaging the background and of removing the contribution of discrete sources down to equivalent point source flux levels of $\sim 10^{-13}$ ergs s^{-1} cm^{-2}. In this respect the data in this work allow us to improve our understanding of the origin of the X-ray background.

The second of these galaxy-related components shows up in the *Einstein* observations as well (as noted at the beginning of this section; cf. Fig. 3). To make this point more clearly, Figure 7*a* shows the background count rate distribution in the Galactic ridge region (Region 1; cf. Fig. 4*a*) to be compared with the corresponding distribution for the canonical featureless Region 4c, shown in Figure 4*b*. The intrinsic mean intensity (i.e., emission in excess of Region 4c), is $\approx 0.88 \pm 0.09 \times 10^{-4}$ counts arcmin^{-2} s^{-1}, i.e., its amplitude is $\sim 23\%$ of the measured background in the featureless Region 4c. Not only is there excess emission in the ridge region, but as we shall show below, the spectrum of this excess emission gives a strong hint for its origins. Our data also show clearly that the ridge is not present at energies below 0.33 keV, confirming the earlier Wisconsin results (Nousek et al. 1982; Sanders et al. 1983). In the present case, it is now very clear that the appearance of the ridge above ~ 0.33 keV is not due to hard Galactic point sources with a flux above 10^{-13} ergs cm^{-2} s^{-1}, since all such sources have been explicitly removed from consideration by virtue of the imaging capabilities of the IPC.

The North Polar Spur.—As for the case of the Galactic ridge, the North Polar Spur (NPS) has been a long-known large-scale feature of the X-ray sky (cf. Bunner et al. 1972; de Korte et al. 1974; Cruddace et al. 1976; Hayakawa et al. 1977). Even earlier, the NPS had been discovered as a feature in the radio sky (cf. Baldwin 1967; Salter 1970), where it has been identified as a possible supernova remnant (cf. Spoelstra 1972; Berkhuijsen 1973; and references therein). By 1971, the prediction had been made that if the NPS were a supernova remnant, then it

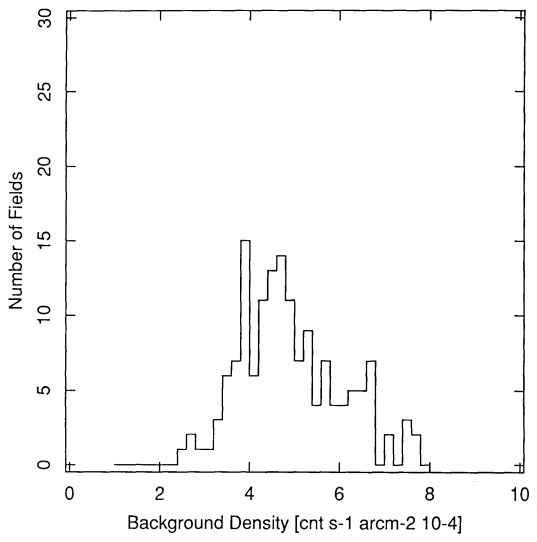

FIG. 7a

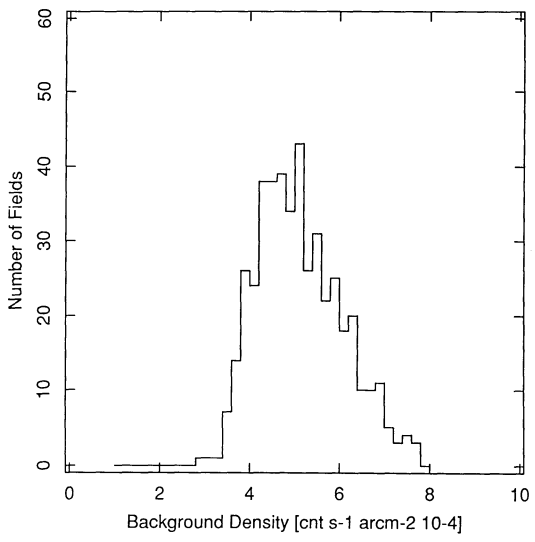

FIG. 7b

FIG. 7.—Comparison of the background count rate distribution functions for (*a*) the Galactic ridge and (*b*) the North Polar Spur. Note that the average count rates for both (*a*) and (*b*) are significantly larger than that for the Region 4c whose distribution is shown in Fig. 4*b* (*solid line*).

ought to be also seen at X-ray wavelengths (Shlovskii & Sheffer 1971); and indeed subsequent rocket observations at these wavelengths led to the by now well-accepted physical association of the regions of nonthermal radio emission and X-ray emission (see references above, as well as the *OSO 8* results reported by Borken & Iwan 1977). Again, this feature can be recognized in the intensity maps of Figure 3, as well as in the background count rate distributions. As an example, we consider here the background count rate map in Figure 7*b*, which can also be compared to the corresponding distribution of the standard comparison region, Region 4c, in Figure 4*b* (*solid line*); this comparison also gives us a mean intensity above the background rate defined by Region 4c of $1.21 \pm 0.05 \times 10^{-4}$ counts arcmin^{-2} s^{-1}, i.e., its excess amplitude is $\sim 31\%$ of the measured background in the featureless Region 4c. As in the case of the Galactic ridge, the spectrum of this discrete component suggests its possible origin; this is briefly discussed further below (cf. § 4.2).

4. SPECTRAL CHARACTERISTICS

The modest ($\Delta E/E \approx 1$ at 1 keV) energy resolution of the IPC also allows one to study the spectral properties of the background. In order to illustrate this capability, we show in Figures 8 and 9 (Plates 13–14) the appearance of the X-ray sky in the soft (0.16–0.8 keV) and hard (0.8–3.5 keV) bands, respectively, using intensity-color maps; both figures were constructed similarly to Figure 3, in four quartiles of the intensity distribution, but now segregated into these two energy bands. These figures show that the background structures discussed above have a clear energy dependence. Furthermore, we present in Figure 10 (Plate 15) a false-color map of the spatial distribution of hardness ratio (HR) in the four quartile of the HR distribution, where HR is defined as the ratio between the background intensity in the (0.8–3.5) keV and (0.16–0.8) keV energy bands. This map clearly shows a distinct hardening of the background spectrum as one approaches the Galactic plane, as one would expect if the majority of observed emission is of nonlocal origin.

4.1. *General Spectral Characteristics*

In order to discuss the spectrum of any given feature in the background, we must first focus on the nature of the spectrum of the featureless comparison region, Region 4c; the median of measured IPC spectra in this region is shown in Figure 11. The error bars shown in Figure 11, computed with a bootstrap procedure, represent the 1 σ uncertainty on median values. We expect that this median spectrum contains, in addition to the signal of the true background itself, two additional components: the particle background and the background due to the internal calibration source; the details of these components, and of the analysis necessary to remove them from the background itself, are discussed in full in Appendix B. In Table 2 we summarize our best estimate both for the nonastrophysical and for the astrophysical background. The data

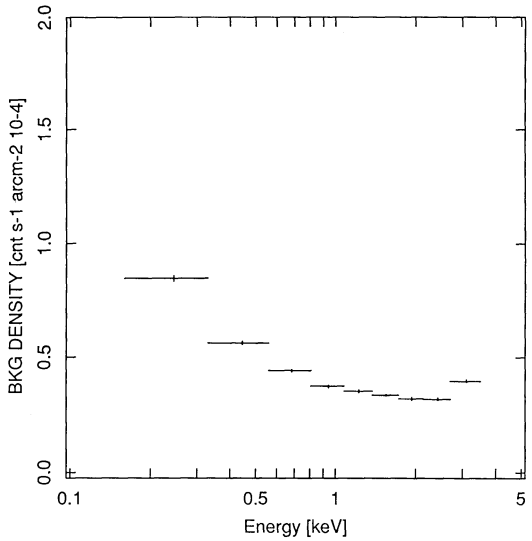

FIG. 11.—The observed IPC spectrum of the background seen in Region 4c, which we use as the canonical comparison. The details of the derivation of this spectrum are discussed in Appendix A.

TABLE 2

OUR BEST ESTIMATES OF PARTICLE-CALIBRATION SOURCE AND REGION 4c ASTROPHYSICAL BACKGROUND SPECTRA

PI Channel	Nonastrophysical Background (counts s^{-1} $arcmin^{-2}$ $\times 10^{-5}$)	Astrophysical Background (counts s^{-1} $arcmin^{-2}$ $\times 10^{-5}$)
2	4.9 ± 1.6	4.0 ± 2.1
3	1.7 ± 1.0	4.2 ± 1.3
4	0.0 ± 1.1	6.6 ± 1.5
5	0.4 ± 0.6	4.0 ± 0.8
6	0.9 ± 0.5	2.8 ± 0.7
7	0.0 ± 0.9	4.2 ± 1.2
8	0.0 ± 0.4	3.6 ± 0.5
9	1.6 ± 0.3	2.0 ± 0.5

NOTE.—Quoted error bars represent formal errors resulting from the adopted fitting procedure; they are due to uncertainty on estimates of particle and calibration source contributions. Note that due to our limited knowledge of systematic effects, the absolute values for channel 10 cannot be reliably computed. A detailed discussion of the table content is presented in Appendix B.

in hand cannot be used to directly determine the spectrum of the isotropic component of the background with very high precision, due to the uncertainty in the nonastrophysical component determination (cf. Appendix B). We have therefore approached the question of the spectrum in two ways: first, as for the actual mean background rate of the background discussed in the previous section, we take the spectrum of the featureless Region 4c as the standard and determine the spectra of spatially discrete background features by subtracting the spectrum of Region 4c from those of the regions under study. This procedure amounts to the assumption that the background seen in Region 4c is the isotropic component (as strongly indicated by the lack of spatial features on small angular size; cf. § 3.2), and hence present in all other Regions, and that the contamination from on-board calibration source and particle events does not change. This procedure of subtracting the Region 4c spectrum results in a corrected background spectrum, which we believe represents the best approximation which can be obtained from the *Einstein* data of individual background components.

The second method of examining the background spectrum is based on an evaluation of the particle background and calibration source contributions to the X-ray background in the aforementioned, least-contaminated by other X-ray features, Region 4c. The precise methods used are discussed in some detail in Appendix B; here we want to point out that due to our limited knowledge of the systematic effects in evaluating the calibration source contribution above 2.7 keV (i.e., in the last PI channel we have considered) we quote the absolute value of X-ray spectrum in Region 4c only in the (0.16–2.7) keV energy range. For present purposes, we shall only require the final result, namely that the median astrophysical background intensity in the 0.16–2.7 keV energy band is 3.14×10^{-4} counts $arcmin^{-2}$ s^{-1} and that the resulting X-ray spectrum, after deconvolving the IPC spectral response, is quite flat over most of the energy range examined (0.16–2.7 keV), at a mean level of ≈ 19 keV cm^{-2} s^{-1} keV^{-1} sr^{-1} in Region 4c; the departures from this flat spectrum will be discussed further in § 5.

4.2. *Spectral Characterization of the Galactic Ridge and the North Pole Spur*

We have studied the relative spectral characteristics of the two major features seen in our maps: the Galactic ridge and the North Polar Spur. Examination of the spatial variation of the corrected background spectrum via the soft and hard false-color maps reveal a distinct hardening of the IPC spectra nearer the Galactic plane (cf. also Fig. 10), with the effect most prominent at the highest background intensity values. Our data are consistent with the idea that the diffuse Galactic component is intrinsically softer than the extragalactic component, but no matter what the nature of the dominant emission component near the Galactic ridge, absorption (roughly below the carbon edge) by cold matter in the disk will cause the emission to *appear* relatively hard, while emission from hot matter well above the disk should show no such extinction.

These assertions can be demonstrated directly by comparing the mean IPC pulse height spectrum of the galactic ridge (Region 1; Fig. 12*a*) with the corresponding spectra of the North Polar Spur (Fig. 12*c*): thus, while the Galactic ridge spectrum is hard, but shows a very distinct cutoff at low photon energies, the North Polar Spur in contrast shows a rather soft spectrum, with no evidence whatsoever for a low-energy cutoff.

The North Polar Spur.—The soft nature of the North Polar Spur (Fig. 12*c*) is consistent with previous determinations of the temperature of the emitting gas based on measurements taken in an energy passband similar to that of *Einstein* (cf. Borken & Iwan 1977) and is also consistent with IPC observations of known supernova remnants (Seward 1989). The spectrum thus supports the standard explanation for this X-ray feature—namely, that it is due to emission from a fairly nearby supernova remnant (see Borken & Iwan 1977; Hayakawa et al. 1977; and references therein). This is strongly indicated also by the direct comparison (cf. Fig. 12*c*) of NPS excess spectrum with the analogous excess spectrum of the Cygnus Loop deduced by the standard annulus background rate normalized to the excess intensity observed in the NPS.

The Galactic ridge.—The origin of the Galactic ridge feature has been subject to some dispute (cf. Kahn & Caillault 1986 for a review). In order to shed some light on this subject in a way not heretofore attempted, we have studied the spectrum of Regions 1 and 2 in Figure 4*a* in some detail. Figure 13*a* gives the first hint about this component's origin: we compare the fractional distribution of mean background count rates for fields in Regions 1 and 2 which are known to contain stellar associations (*solid line*) with the corresponding distribution for fields in Regions 1 and 2 which are not known to contain

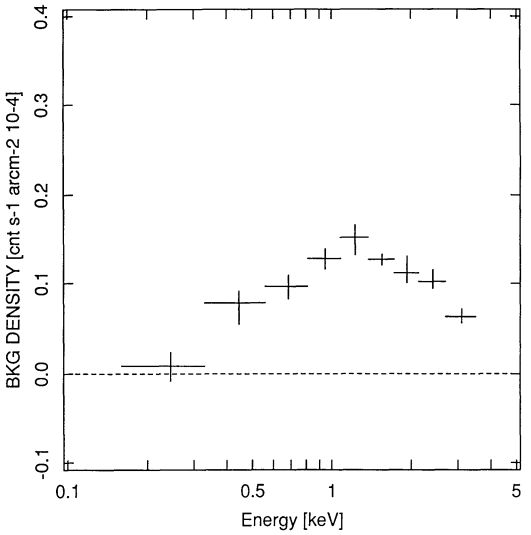

FIG. 12*a*

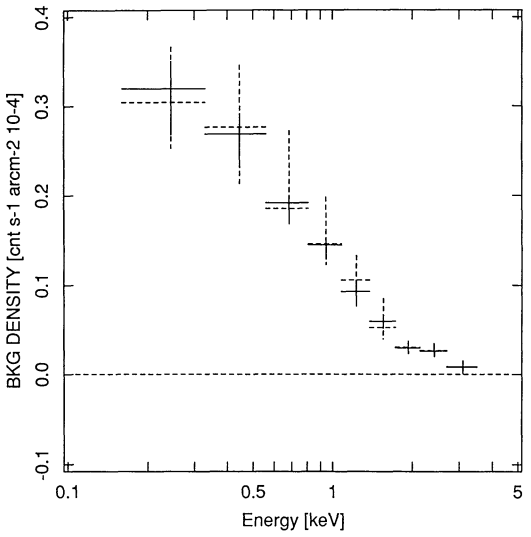

FIG. 12*c*

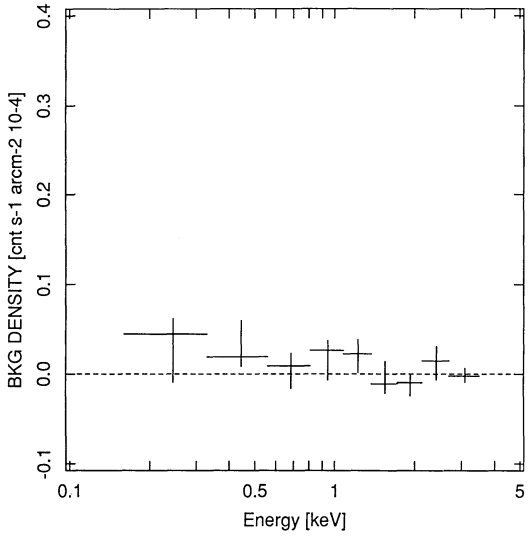

FIG. 12*b*

FIG. 12.—Comparison of the corrected IPC spectra for (*a*) the Galactic ridge, (*b*) the Galactic anticenter region (Region 2 in Fig. 4*a*), and (*c*) the North Polar Spur (*solid line*) compared to the normalized excess spectrum of the Cygnus Loop (*dashed line*). In all cases, the correction was made by subtracting out the observed IPC spectrum obtained from the featureless canonical comparison region, Region 4c, shown in Fig. 11.

stellar associations (*dashed line*); the selection of fields with and without associations was based on the compilations published by Alter, Ruprecht, & Vanysek (1970) and Ruprecht, Balazs, & White (1981). This comparison suggests that the Galactic ridge is largely attributable to the fields containing stellar associations (including open clusters and regions of star formation). More quantitatively, a Kolmogorov-Smirnov two-sample test shows these two distributions differ at better than the "3 σ" level (i.e., the null hypothesis that the two distributions are drawn from the same parent population is rejected at the 0.9993 confidence level).

Yet more telling is a direct comparison of the IPC spectra: Figure 13*b* compares the corrected IPC spectrum of the background for the IPC Galactic ridge fields containing associations with the median IPC spectrum for the X-ray sources detected in those *Einstein* images falling in Region 1 and 2 (Fig. 4*a*) containing stellar cluster or associations. We have considered only the X-ray sources detected in the broad band with the local method (cf. Harnden et al. 1984), unobscured by the IPC entrance window support structure or edges, and with count rate less than 0.1 counts s^{-1} to exclude high rate sources that could affect the results. The similarity of these two IPC spectra is striking. This evidence, taken together with the previous statistical test on the distributions shown in Figure 13*a*, argues forcefully that the excess Galactic ridge emission is largely due to nothing else but the unresolved contribution from discrete sources lying within stellar associations in the Galactic disk, as well as from other discrete sources near the Galactic plane whose spectra are similar to those of stars in such associations, e.g., young, active stars. Furthermore, the additional extinction at the lower energies due to absorption by intervening gas in the disk should make this unresolved disk component appear yet harder than the emission from the sources in the more nearby associations—and the spectral comparison of Figure 13*b* is consistent with this idea. Other possible contributors include active M dwarfs (cf. Rosner et al. 1981; Schmitt & Snowden 1990; Kashyap et al. 1991)—which are a numerous stellar type, and which are known to have relatively hard stellar X-ray spectra (Schmitt et al. 1990) and young compact OB associations which also have the requisite, relatively hard, spectrum (cf. Chlebowski, Harnden, & Sciortino 1989); in the latter case, the relatively sparse distribution of OB associations suggests, however, that these objects cannot be a very significant contributor. A more detailed modeling of these contributions to the ridge will be discussed elsewhere (Micela et al. 1991).

We cannot of course exclude modest additional contributions from sources which have in the past been suggested as significant contributors, but are not normally associated with star clusters (such as white dwarf binaries and RS CVn stars, Worrall et al. 1982; young supernova remnants, Koyama et al 1986a; and very old supernova remnants, Sanders et al. 1983); but our results indicate that these additional contributions cannot dominate the Galactic ridge component—none of these alternative contributors can readily account for the data shown in Figures 13*a* and 13*b* and the other characteristics

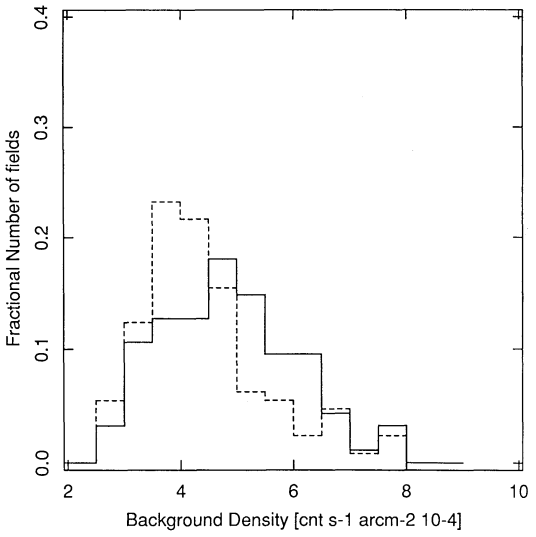

FIG. 13a

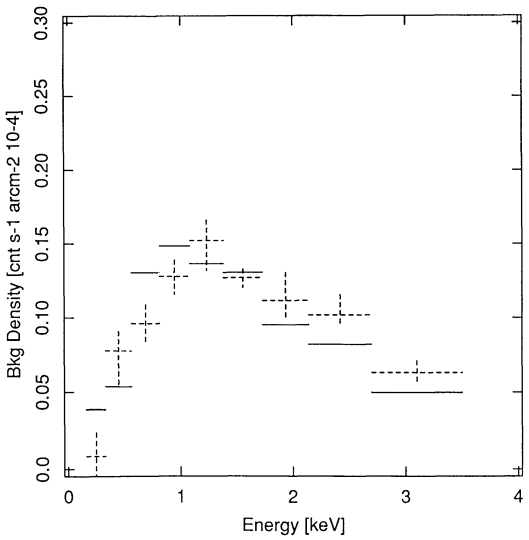

FIG. 13b

FIG. 13.—(*a*) Comparison of the background count rate fractional distribution functions for 94 IPC fields lying in the Galactic plane which were pointed at stellar associations in Regions 1 and 2 of Fig. 4*a* (*solid line*), and the sample of 129 IPC fields lying in these regions from which pointings at stellar associations were excluded (*dashed line*). (*b*) Comparison of the corrected IPC spectrum for the Galactic ridge with the median IPC spectrum of X-ray detections of point sources lying in stellar associations; the latter spectrum has been normalized so as to have the same mean background count rate (in counts arcmin^{-2} s^{-1}) in IPC channels 2–10 as the median background count rate for fields lying in the Galactic ridge region.

discussed. In particular, the white dwarfs as a class are not likely contributors due to their observed soft spectrum; and a similar argument applies to the supernova remnants. The RS CVn stars are not likely contributors due to their low space density (which prevents them from accounting for more than 10% of the observed ridge intensity) and scale height of a few hundred parsecs (which prevent them from accounting for the observed thickness of the Galactic ridge).

We thus conclude, based on all available evidence, that the Galactic ridge is due to excess emission from stars in young associations. Further, we predict that similar ridges will be present in spatially resolved X-ray images of external spiral galaxies seen edge-on once strong sources such as low- and high-mass X-ray binaries are removed. If our results are borne out, then such observations would furnish a reliable measure of extreme Population I late-type stars in external galaxies for which presently there are not strong experimental constraints.

5. THE SPECTRUM OF THE ISOTROPIC COMPONENT: THE GALACTIC AND EXTRAGALACTIC BACKGROUND

Table 3 provides a summary of our results for the mean diffuse soft X-ray background level as a function of energy as measured in Region 4c, based on the discussion of Appendix B, as well as a comparison to the extrapolated extragalactic background, based on the classic power-law relation (assuming no absorption; Tucker & Schwartz 1986).

$$\frac{dI}{dE}(2.0\text{–}10\ \text{keV}) = 7.7E^{-0.4}\ \text{keV cm}^{-2}\ \text{s}^{-1}\ \text{sr}^{-1}\ \text{keV}^{-1}\ . \quad (1)$$

The absolute fluxes in Table 3 have been computed assuming a power law with the "canonial" spectral index $\alpha = 0.4$ and $\log N_H = 18$. In computing them we have taken advantage of using Pulse-height Independent (PI) channels and have used a program (FINSPEC) developed at CfA, that takes into account available calibration of IPC spectral response, and evaluates, for each PI channel, the conversion factor from count rates to flux. We have also verified that for α ranging between 0 and 0.8 the deduced fluxes change at most by 10%.

Table 4 and Figure 14 provide a summary of representative previous measurements of the background in similar energy ranges. Three results immediately follow from these comparisons: First, our results are consistent with previous direct mea-

TABLE 3

OUR BEST ESTIMATE FOR THE SPECTRUM OF THE DIFFUSE BACKGROUND (MEAN FLUXES FOR REGION 4c)

PI CHANNEL	⟨E⟩ (keV)	OBSERVED FLUX (cm^{-2} s^{-1} sr^{-1} keV^{-1})	(× 10^{-8} ergs cm^{-2} s^{-1} sr^{-1} keV^{-1})	(keV cm^{-2} s^{-1} sr^{-1} keV^{-1})	PREDICTED FLUX (Eq. [1]) (keV cm^{-2} s^{-1} sr^{-1} keV^{-1})
2	0.25	104.6 ± 53%	4.10	25.6	13.5
3	0.45	52.6 ± 31	3.75	23.4	10.6
4	0.69	39.2 ± 23	4.35	27.2	8.9
5	0.95	20.3 ± 20	3.09	19.3	7.9
6	1.23	10.4 ± 25	2.04	12.8	7.1
7	1.56	12.4 ± 29	3.10	19.4	6.5
8	1.94	8.9 ± 14	2.78	17.4	5.9
9	2.42	4.6 ± 25	1.80	11.3	5.4

NOTE.—Percentage errors are due to the uncertainty on determination of particle and calibration source contributions. This uncertainty dominates error estimates. The spectrum has been evaluated assuming a power-law spectrum with index $\alpha = 0.4$ and $\log N_H = 18$.

TABLE 4

SOME COMPARISONS WITH PREVIOUS MEASUREMENTS

Bandpass (keV)	Direction (l, b)	Flux (cm^{-2} s^{-1} sr^{-1} keV^{-1})	Reference
0.16–0.33	(Region 4c)	105	1
0.33–1.2	(Region 4c)	37	1
1.5–2.7	(Region 4c)	12	1
0.15–0.3	(10°–30°, 40°–60°)	107	2
0.15–0.3	(10°–30°, 5°–30°)	70	2
0.3–1.2	(10°–30°, 40°–60°)	27	2
0.3–1.2	(10°–30°, 5°–30°)	32	2
@10	(60°, ~0°)	$6–8 \times 10^{-2}$	3

REFERENCES.—(1) This work; (2) de Korte et al. 1974; (3) Worrall et al. 1982.

surements of the diffuse background in the approximate energy range 0.2–3.0 keV based on instruments with far inferior angular resolution and without the capability of subtracting the contributions of discrete sources up to a given flux limit. This conclusion serves to reinforce our contention that we have indeed measured the true diffuse X-ray background in the IPC energy bandpass and is generally consistent with the very recent diffuse background determination of Wu et al. (1990; see their Fig. 6), based on a smaller number of IPC fields and a different analysis technique. Second, our spectrum is substantially in excess of the measured extragalactic contribution extrapolated to our passband; alternatively, extrapolation of our result to higher energies would substantially exceed the observed background at these higher energies—so that whatever processes contribute to the background in our energy range must sharply cut off at energies above ≈3–4 keV. Third, there is significant evidence for a soft cutoff in our spectrum shown in Figure 14, suggesting that a significant amount of

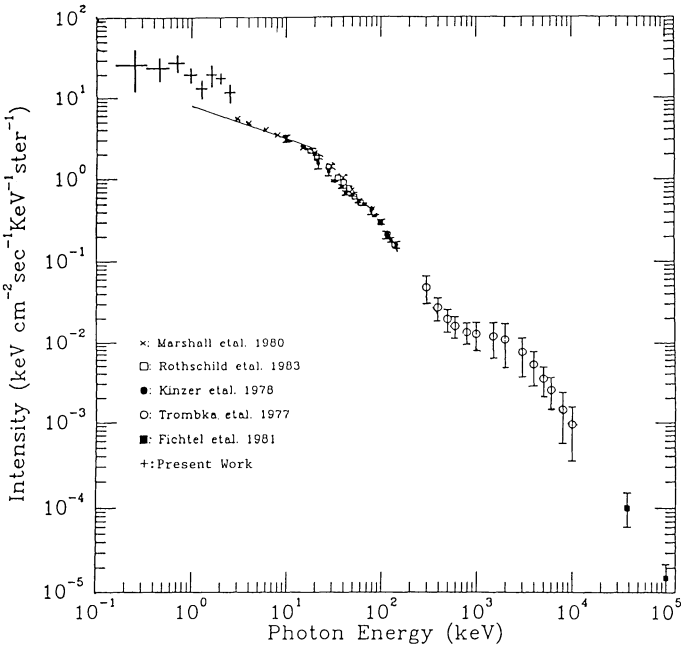

FIG. 14.—Comparison of the previous measurements of the diffuse X-ray background (adapted from Schwartz, Qian, & Tucker 1989) with the measured spectrum in the (0.16–2.7) keV range (this paper) from Region 4c, and with past best-fit models for AGNs in the (3–10) keV energy range (from Tucker & Schwartz 1986). The details of the derivation of absolute fluxes are discussed in Appendix B and in § 5.

absorption intervenes between us and whatever the ultimate source of these X-rays proves to be

Consider the make-up of the "softer channel" background in Region 4c, when the particle contribution—ranging, as listed in Table 2, between 60% and 30%—has been removed. At least two contributors can be identified;

1. The first is the stellar contribution to the Galactic component of the diffuse X-ray background unresolved by the IPC. Model calculations based on the maximum likelihood X-ray luminosity functions for stars derived from the *Einstein* observations (Rosner et al. 1981) yield flux values of 3.1×10^{-9} ergs cm^{-2} s^{-1} sr^{-1} keV^{-1} in the energy range 0.16–0.28 keV (i.e., ~8% of "astrophysical" background measured in Region 4c in channel 2 of IPC), and 3.5×10^{-9} ergs cm^{-2} s^{-1} sr^{-1} keV^{-1} in the energy range 0.28–1.0 keV (i.e., ~9% of value measured in channels 3–5), all at a Galactic longitude of 30°. Schmitt & Snowden (1990), adopting a description of stellar coronal emission spectra in terms of a continuous emission measure distribution and the mean value of nearby dwarf M stars X-ray luminosity, have estimated a negligible stellar contribution in the C band, and stellar contributions in the M1 and M2 band that at the minimum are ~3% and ~5% of present determination, respectively. More recently Kashyap et al. (1991) have performed a new detailed calculation of stellar contribution to the diffuse soft X-ray background adopting a two-temperature description of stellar spectra with the ratio of emission measure being a function of stellar X-ray luminosity, and taking into account published maximum likelihood X-ray luminosity functions for nearby stars derived from the *Einstein* observations. The stellar contribution in the C band predicted by Kashyap et al. (1991) is 2%–3% of Region 4c background intensity in the same energy range, and ~9% in the M1, M2, and M0 bands. All these calculations indicate that stars do contribute to the Galactic component of the diffuse M band X-ray background.

2. The second is an undetermined "astrophysical" component, accounting for ~50% of the measured soft background. This last component shows a trend of decreasing intensity with decreasing Galactic latitude, as previously observed in the "C-band" data (cf. the review of McCammon & Sanders 1990, and references therein cited).

What can the 0.16–2.7 keV diffuse background be attributed to? The "standard" contributors to the Galactic diffuse background—diffuse local hot gas, stars, supernova remnants, and Galactic halo gas—potentially all satisfy the first two constraints: that is, it is possible to assemble a mix of these contributors which results in the spectral shape of the diffuse background we see *above* channel 2 (i.e., above ≈0.3 keV). The key problem is the soft cutoff seen in the lowest channels we have considered: we cannot see any way of inserting sufficient Galactic absorbing matter (e.g., N_H in excess of 10^{21} cm^{-2}) at relatively high Galactic latitudes, and rather uniformly, as required by the spectrum seen in Region 4c in such a way that sources associated with our Galaxy will yield the observed cutoff spectrum. Thus, unless we have neglected some as yet unknown effect in our analysis of the IPC spectrum, or an as yet unknown class of Galactic contributors with the proper scale height, density, and spectrum so to generate the measured cutoff spectrum, our observations suggest strongly that, above ~0.3 keV, the spectrum evaluated in Region 4c, when the contribution of stellar sources is removed in the soft channels, is due to extragalactic emission.

Indeed, the above constraints suggest an obvious form for

the spectrum of the extragalactic diffuse emission: If the emission is due to thermal emission from a hot gas at a temperature T in the 3–4 keV range, then the exponential cutoff (at $E/kT \approx 1$) will ensure that the spectrum of the diffuse emission above the *Einstein* bandpass remains unaffected. One example of a candidate for such emission is the hot gas in halos surrounding galaxies and clusters of galaxies (Schaeffer & Silk 1988); however, recently, Evrard & Henry (1991) have computed that expected cluster source contribution is no more than 10% of the observed soft X-ray background. Another example is the class of discrete X-ray sources associated with active galactic nuclei (AGNs) (we do not distinguish between active galaxies such as Seyferts and quasars; Giacconi et al. 1979b; Tananbaum et al. 1979; Maccacaro, Gioia, & Stocke 1984). Recently some authors (Qian 1989; Schwartz, Qian, & Tucker 1989) have proposed a solution to the so-called spectral paradox, i.e., the difficulty of synthesizing the measured spectrum of the diffuse X-ray background starting from simple power-law description of AGN spectra. These authors have shown that the IPC spectra of AGNs can be described very well either with a log Gaussian or a power-law plus thermal bremsstrahlung shape, and that models consisting of superpositions of such spectra closely reproduce the slope of the X-ray background spectrum in the 3–12 keV energy range. Note that the correlation analysis we discussed earlier is consistent with AGNs as a significant contributor class. Recently, Rogers & Field (1991) adopting a modified version of the model of Fabian et al. (1990) for the cosmic X-ray background, in which the emission is due to AGNs at large redshifts, have predicted, in qualitative agreement with present paper results, that the intensity of the X-ray background below 3 keV is significantly above that extrapolated from observation above 3 keV (cf. eq. [1]). However, their prediction falls below the measured X-ray background intensities at 1 keV resulting from present work.

To conclude, we have addressed the important question as to what extent the extragalactic background contributes within the passband we are considering: Region 4c—the region least affected by emission obviously associated with our Galaxy—is clearly the place where this question is best posed; and our results suggest that most of the flux we observe above ~ 0.3 keV in this region is indeed extragalactic.

6. SUMMARY AND CONCLUSIONS

We have analyzed the complete set of Imaging Proportional Counter pointings from the *Einstein Observatory*, with the aim of characterizing the diffuse soft X-ray background on angular scales of order of a degree and larger. Each one of 1633 $1^\circ \times 1^\circ$ IPC fields, selected for low contaminant effects, was used to generate a measurement of the background, leading to a survey of roughly 5% of the sky, and a map of the background sky intensity in the *Einstein* energy passband of 0.16–3.5 keV. This map shows a general correspondence to features seen at higher energies (such as the Galactic ridge) and provides a picture of the sky at low photon energies with angular resolution higher than previously possible. We are able to confirm that the Galactic ridge is seen at photon energies above ~ 0.3 keV, but not below 0.3 keV. Analysis of our data further shows that the observed fluctuations in the mean count rate in the $1^\circ \times 1^\circ$ fields cannot be accounted for by purely statistical effects; but autocorrelation analysis also shows that on angular scales much larger than 10°, the diffuse X-ray background as seen by *Einstein* is rather smooth when known features are excluded. This implies that the diffuse background must be structured on angular scales somewhat larger than 1°, an angular scale which our data do not sample sufficiently well for us to study directly. Such a study should be eminently feasible with the *ROSAT* mission.

We also took advantage of the energy resolution of the IPC in order to construct maps of the background sorted by photon energy. One interesting result is that we find a distinct hardening of the background spectrum as one approaches the Galactic plane, a trend particularly striking in maps made for the highest quartile in background intensity; this hardening turns out on closer inspection to be principally due to a significant cutoff at low energies, presumably due to substantial absorption by cold matter lying in the Galactic disk. More detailed study of the spectral characteristics of the Galactic ridge in fact suggests very strongly that the excess emission is due to contributions from young active stars, such as low-mass stars in stellar associations, and that contributions from other types of sources suggested earlier as significant contributors—such as supernova remnants, white dwarf binaries, and RS CVn stars—cannot readily account for the spectral characteristics of this excess. We also find that the spectral characteristics of the other main discrete structure visible in our maps, namely the North Polar Spur, is significantly softer than the Galactic ridge, and shows no evidence for extinction at low energies; this is consistent with the idea that the NPS emission is due to a relatively nearby supernova shell, as strongly indicated by the direct comparison of NPS excess spectrum with the analogous excess spectrum of the Cygnus Loop.

Finally, we have been able to estimate the true spectrum of the diffuse background as seen by the IPC; this spectrum shows a substantial excess in emission over the extrapolations of the diffuse spectrum above 3 keV into the *Einstein* passband. The rather flat nature of this spectrum above 0.5 keV, the cutoff required between 3–4 keV in order to satisfy the observed spectrum above the *Einstein* passband, and the cutoff seen in the lowest IPC channel we can confidently analyze, when taken together, suggest that the source of this diffuse emission is a thermal spectrum with a temperature T in the 1–4 keV range, whose source must lie well outside our Galaxy. Cluster halo gas seems to be one plausible candidate for this emission, but based on the results of angular correlation analyses we have performed, the possibility of a significant contribution of AGNs must also be entertained (see also De Zotti et al. 1990).

The success of the present effort in characterizing the diffuse soft X-ray background—despite the fact that the *Einstein* IPC and its analysis software were not at all designed to study the diffuse background in the way we have—strongly suggests that future imaging missions, principally the ongoing *ROSAT* mission and forthcoming *AXAF* and other X-ray telescopes, should plan from the outset to use the normal background data for diffuse background studies. The *ROSAT* mission in particular will offer an unprecedented opportunity of studying the least understood component of the diffuse soft X-ray background, namely that associated with the 0.3–1.0 keV M band, and will very likely allow us to disentangle the contributions of young stars, especially those within associations, from other likely contributors.

This work has been partially supported by Agenzia Spaziale Italiana (ASI) and Italian Ministero della Università e della Ricerca Scientifica e Tecnologica (G. S. V., S. S., G. M.) and

IAIF–CNR (G. S. V.), the Smithsonian Institution (R. R.), and NASA (F. R. H., R. R., G. S. V.). We acknowledge useful comments of D. Harris, P. Henry, E. Kellogg, S. Serio, H. Tananbaum, and of one anonymous referee which have allowed us to improve our presentation. This work is part of the Ph.D. thesis of G. M.

APPENDIX A

DETERMINATION OF THE IPC ANNULAR BACKGROUND RATE

The ReV-1B processing system (Harnden et al. 1984) routinely determined a field background rate for all IPC images as the first step in the process of automated source detection. However, since the computed value was intended only as a description of the *total* diffuse emission present in the field, regardless of its origin, it cannot be used to infer cosmic background rates without further refinements.

The image region used to compute the background value, an annulus with inner and outer radii of 8′ and 15′, was routinely screened to eliminate contributions from discrete, pointlike sources appearing within it, by iterative application of an algorithm that divided the annulus into cells and discarded those with count rates widely discrepant from the mean. Other information supplied by the ReV-1B processing (viz, quantities derived as part of the XDETECT algorithm, cf. Tables 19, 21, and 22 of Harnden et al. 1984) can be used to help separate unwanted particle and atmospheric components from the total background, leaving the astrophysically interesting information.

Two nonastrophysical background components, due to particle-induced events and to solar X-rays scattered and fluoresced in Earth's atmosphere, were recognized and addressed by the ReV-1B XDETECT algorithm. A third, instrumental component (events induced by the built-in radioactive calibration source) did not require attention in the XDETECT algorithm because it varied only slowly (with the 13.4 yr half-life of the ^{244}Cm radioisotope) but must be addressed when inferring the absolute spectrum of the cosmic background.

ReV-1B processing assessed the first component from simultaneous measurements made with the so-called guard counter (a proportional counter which operated independently of the IPC and was designed to provide anticoincidence rejection of omnidirectional radiation). Those observation spans with particle background rate higher than a fixed threshold are rejected from scientific data processing. Below this threshold, we do not find any correlation between guard rate and imaged background.

The atmospheric component was assessed in ReV-1B processing via a calculation of the geometric configuration ("viewing geometry") of the Sun, Earth, and target, and subsequent classification and flagging of data as "bad," "good," "better," or "best." Although Fink, Schmitt, & Harnden (1988) have done a more accurate and thorough job of computing such solar-induced effects, the treatment employed in ReV-1B is believed to be sufficiently accurate to permit the inference of background rates free of such effects.

We have corrected the ReV-1B field-background values to infer rates obtaining for data flagged as having "best" viewing geometry (VG). In deducing these corrections, we have used XDETECT quantities which give the fractions of image exposure times spent in each VG quality, and the corresponding rates, as a function of energy band. From typical images containing a mix of good, better, and best VG data, we rejected those which had overall background rates that is higher, above 1 σ level, than the rates obtained during the VG-best intervals that contributed to the individual images. In this way, we screened out cases for which our correction procedure might have been less successful.

We have also eliminated the fields with extended or strong point sources, namely all those fields pointed in the direction of known supernova remnants, such as Vela, Cygnus, Crab, Cas A, etc., clusters of galaxies, and the Large and Small Magellanic Clouds. Furthermore, we have rejected all the fields containing sources having a rate greater than 0.5 counts s^{-1}.

Finally, we also eliminated images with very short exposures (less than 500 s) since statistical fluctuations are large in such cases.

APPENDIX B

EVALUATION OF THE IPC PARTICLE-BACKGROUND SPECTRUM

In order to determine the characteristics of the "true" astrophysical background, we had to evaluate the spectrum and the overall intensity of the non–X-ray events attributable to (*i*) "leakage" from the IPC calibration source (cf. Appendix A) and to (*ii*) interactions induced by the in-orbit particle flux. These contributions occur in two rather different energy ranges, with calibration source events dominating the observed IPC spectrum at energies above 2 keV, and particle-induced events, at energies below (Harnden et al. 1984).

We have initially attempted to determine the spectrum contributed by calibration-source "leakage" by comparing two images centered on the same region of the sky but taken with and without the aluminum filter (sequences 10754 and 10755, respectively). When inserted in the optical path (Giacconi et al. 1979a), this filter essentially eliminated X-ray photons above 2 keV, thereby permitting, in principle, an absolute determination of the calibration source spectrum. Unfortunately, the image with the filter was obtained on a day in which the solar activity (as measured by the value of planetary Kp index, namely a world-wide solar magnetic activity index) was particularly high. Hence this observation was somewhat contaminated and cannot be used to evaluate the absolute spectrum of calibration source "leakage."

Due to this problem, we have been forced to determine the spectrum of all the nonastrophysical events (i.e., particle and

calibration leak events) by assuming that the radial distribution of the background counts can be described as the superposition of two components with distinct spatial signatures: (1) a spatially uniform nonastrophysical component and (2) a "true" X-ray component that decreases with increasing off-axis angles due to mirror vignetting (see also Wu et al. 1990). Background counts for this purpose were collected from the standard 5′–6′ background annuli of detected, ReV-1B sources which had count rates smaller than 0.05 counts s^{-1}, which were unobscured by the IPC entrance window support structure, and which fell in the IPC images of Region 4c (cf. Fig. 4*a*) used in the present study.

Restricting our analysis to radial distances between 6′ and 28′ and adopting the energy-dependent vignetting functions given by Harnden et al. (1984), we determined the intensities of the nonastrophysical contribution in each of the eight Pulse-height Independent (PI; cf. Harnden et al. 1984) bins corresponding to the energy band (0.16–2.7) keV, fitting for each PI bin the sum of a uniform component and of a vignetted component to the radial distribution of data. This fitting procedure allows us to determine also formal errors for all the deduced quantities (cf. Table 2).

The assumption of a flat, particle-induced distribution is clearly a simplification: a dramatic increase in the relative number of particle to X-ray events is known to occur at the physical borders of the IPC. To overcome this problem, ReV-1B masked out all events falling closer than 7′.5 to any detector edge, thereby retaining only the central $1° \times 1°$ of each IPC image. The particle flux in this central region is indeed quite uniform, and we are confident that the nonastrophysical event rates below 2 keV (i.e., up to PI channel 8), largely due to particle-induced events, derived above provide a reasonable estimate. On the contrary, the assumption of a flat spatial distribution for the calibration leak events results to be an unsatisfactory approximation above ~ 3 keV when these events start to become a significant contributor. Our limited knowledge of the real spatial distribution of calibration source leak prevents us from properly evaluating the contribution of nonastrophysical events starting from PI channel 10. Hence, we have restricted our determination of absolute X-ray background spectrum to the (0.16–2.7) keV energy range.

The mean contribution of non–X-ray events so derived is $(0.95 \pm 0.25) \times 10^{-4}$ counts $\mathrm{arcmin}^{-2}\ \mathrm{s}^{-1}$ in the 0.16–2.7 keV energy band.

Our best estimate of the spectra of the "nonastrophysical background," namely particle and calibration source contribution, is given in Table 2, together with the deduced "astrophysical background."

Finally, in order to estimate the success of our screening procedure, we have considered 119 pairs of IPC fields pointed at the same sky regions (inside 0°.5); for each of them we have computed the absolute value of the difference in measured IPC background, and finally we have determined the 1 σ point of the distribution of these absolute values, that should be associated with any residual variations due to (uncorrected) fluorescent emission and particle-induced flux contributions. The result of this analysis shows that no more than 19% of the observed variance in the background-density distributions (cf. Fig. 2) can be accounted for by the above effect.

REFERENCES

Alter, G., Ruprecht, J., & Vanyzek, V., eds. 1970, Catalog of Star Clusters and Associations (Budapest: Akademiai Kiado)
Barcons, X., & Fabian, A. C. 1989, MNRAS, 237, 119
Baldwin, J. D. 1967, in Radio Astronomy and the Galactic System, ed. H. van Woerden (New York: Academic)
Berkhuijsen, E. M. 1973, A&A, 24, 143
Bleach, R. D., Boldt, E. A., Holt, S. S., Schwartz, D. A., & Serlemitsos, P. J. 1972, ApJ, 174, L101
Boldt, E. et al. 1979, in X-ray Astronomy, ed. W. A. Baity & L. E. Peterson (Oxford: Pergamon Press), 433
Borken, R. J., & Iwan, D. C. 1977, ApJ, 218, 511
Bunner, A. N., Coleman, P. L., Kraushaar, W. L., & McCammon, D. 1972, ApJ, 172, L67
Chambers, J. M., Cleveland, W. S., Kleiner, B., & Tukey, P. A. 1983, Graphical Methods for Data Analysis (Belmont, CA: Wadsworth International Group)
Chlebowski, T., Harnden, F. R., Jr., & Sciortino, S. 1989, ApJ, 341, 427
Cruddace, R. G., Friedman, H., Fritz, G., & Shulman, S. 1976, ApJ, 207, 888
de Korte, P. A. J., Bleeker, J. A. M., Deerenberg, A. J. M., Tanaka, Y., & Yamashita, K. 1974, ApJ, 190, L5
De Zotti, G., Persic, M., Franceschini, A., Danese, L., Palumbo, G. G. C., Boldt, E. A., & Marshall, F. E. 1990, ApJ, 351, 22
Edelson, R. A., & Krolik, J. H. 1988, ApJ, 333, 646
Evrard, A. E., & Henry, J. P. 1991, ApJ, submitted
Fink, H. H., Schmitt, J. H. M. M., & Harnden, F. R., Jr. 1988, A&A, 193, 345
Fabian, A. C., George, I. M., Miyoshi, S., & Rees, M. J. 1990, MNRAS, 242, 14P
Giacconi, R., Gursky, H., Paolini, F., & Rossi, B. 1962, Phys. Rev. Letters, 9, 439
Giacconi, R., et al. 1979a, ApJ, 230, 540
Giacconi, R., et al. 1979b, ApJ, 234, L1
Gorenstein, P., Harnden, F. R., Jr., & Fabricant, D. G. 1981, IEEE Trans. Nucl. Sci., NS-28, 869
Gorenstein, P., & Tucker, W. H. 1972, ApJ, 176, 333
Griffiths, R. E., et al. 1983, ApJ, 269, 375
Hamilton, T. T., & Helfand, D. J. 1987, ApJ, 318, 93
Harnden, F. R., Jr., Fabricant, D. G., Harris, D. E., & Schwarz, J. 1984, Scientific Specifications of the Data Analysis System for the *Einstein Observatory* (*HEAO 2*) Imaging Proportional Counter (SAO SP-393) (Cambridge: Smithsonian Astrophysical Observatory)
Harnden, F. R., Jr., Sciortino, S., Maggio, A., Micela, G., Vaiana, G. S., Schmitt, J. H. M. M., & Rosner, R. 1990, in Imaging X-ray Astronomy, ed. M. Elvis (Cambridge: Cambridge Univ. Press), 313
Hayakawa, S., Kato, T., Nagase, F., & Yamashita, K. 1979, PASJ, 31, 71
Hayakawa, S., Kato, T., Nagase, F., Yamashita, K., Murakami, T., & Tanaka, Y. 1977, ApJ, 213, L109
Hoaglin, D. C., Mosteller, F., & Tukey, J. W. 1985, Exploring Data Tables, Trends, and Shapes (New York: John Wiley & Sons), chap. 10(c)
Iwan, D., Marshall, F. E., Boldt, E. A., Mushotzky, R. F., Shafer, R. A., & Stottlemyer, A. 1982, ApJ, 260, 111
Kahn, S. M., & Caillault, J.-P. 1986, ApJ, 305, 526
Kahn, S. M., Seward, F. D., Harnden, F. R., Jr., & Gorenstein, P. 1985, ApJ, 299, 821
Kashyap, V., Rosner, R., Micela, G., Sciortino, S., Vaiana, G. S., Harnden, F. R., Jr. 1991, ApJ, submitted
Koyama, K. 1988a, Comments Ap., 12, 287
———. 1988b, ISAS Res. Note, n. 391
Koyama, K., Ikeuchi, S., & Tomisaka, K. 1986a, PASJ, 38, 503
Koyama, K., Makishima, K., Tanaka, Y., & Tsunemi, H. 1986b, PASJ, 38, 121
Kraushaar, W. L. 1979, in X-ray Astronomy, ed. W. A. Baity & L. E. Peterson (Oxford: Pergamon Press), 293
Maccacaro, T., Gioia, I. M., & Stocke, J. T. 1984, ApJ, 283, 486
McCammon, D., Burrows, D. N., Sanders, W. T., & Kraushaar, W. L. 1983, ApJ, 269, 107
McCammon, D., & Sanders, W. T. 1990, ARA&A, 28, 657
Micela, G., Harnden, F. R., Jr., Rosner, R., Sciortino, S., & Vaiana, G. S. 1989a, in AGN and the X-Ray Background, ed. J. Hunt & B. Battrick (Proc. 23rd ESLAB Symposium) (ESA SP-296), 1043
Micela, G., Sciortino, S., Vaiana, G. S., Harnden, F. R., Jr., Rosner, R., & Schmitt, J. H. M. M. 1989b, Mem. Soc. Astr. Italiana, 239, 60
Micela, G., Sciortino, S., Vaiana, G. S., Harnden, F. R., Jr., & Rosner, R. 1990, in Imaging X-Ray Astronomy, ed. M. Elvis (Cambridge: Cambridge Univ. Press), 247
Micela, G., et al. 1991, in preparation
Novsek, J. A., Fried, P. H., Sanders, W. T., & Kraushaar, W. L. 1982, ApJ, 258, 83
Persic, M., De Zotti, G., Boldt, E. A., Marshall, F. E., Danese, L., Franceschini, A., & Palumbo, G. G. C. 1989, ApJ, 336, L47
Primini, F. A., Murray, S. S., Huchra, J., Schild, R., Burg, R., & Giacconi, R. 1991, ApJ, 374, 440

Protheroe, R. J., Wolfendale, A. W., & Wdowczyk, J. 1980, MNRAS, 192, 445
Qian, Y. 1989, Ph.D. thesis, Harvard University
Rogers, R. D., & Field, G. B. 1991, ApJ, 370, L57
Rosner, R., et al. 1981, ApJ, 249, L5
Ruprecht, J., Balazs, B., & White, R. E. eds. 1981, Catalog of Star Clusters and Associations—Supplement (Budapest: Akademiai Kiado)
Salter, C. J. 1970, Ph.D. thesis, Manchester University
Sanders W. T., Burrows, D. N., Kraushaar, W. L., & McCammon, D. 1983, in Supernova Remnants and Their X-Ray Emission, ed. J. Danziger & P. Gorenstein (Dordrecht: Reidel), 361
Schaeffer, R., & Silk. J. 1988, ApJ, 333, 509
Schmitt, J. H. M. M., Collura, A., Sciortino, S., Vaiana, G. S., Harnden, F. R., Jr., & Rosner, R. 1990, ApJ, 365, 704
Schmitt, J. H. M. M., Fink, H., & Harnden, F. R., Jr. 1987, ApJ, 322, 1023
Schmitt, J. H. M. M., & Snowden, S. L. 1990, ApJ, 361, 207
Schwartz, D. A. 1978, in X-ray Astronomy, ed. W. A. Baity & L. E. Peterson (Oxford: Pergamon), 453
Schwartz, D. A., Qian, Y., & Tucker, W. H. 1989, in AGN and the X-Ray Background, ed. J. Hunt & B. Battrick (Proc. 23rd ESLAB Symposium) (ESA SP-296), 1043
Sciortino, S., Harnden, F. R., Jr., Maggio, A., Micela, G., Vaiana, G. S., Schmitt, J. H. M. M., & Rosner, R. 1988, in Astronomy from Large Databases (ESO Conference and Workshop Proceedings 28), ed. F. Murtagh & A. Heck, 483
Seward, F. D. 1989, private communication
Shlovskii, I. S., & Sheffer, E. K. 1971, Nature, 231, 173
Spoelstra, T. A. Th. 1972, A&A, 21, 61
Tananbaum, H. D., et al. 1979, ApJ, 234, L9
Tucker, W. H., & Schwartz, D. A. 1986, ApJ, 308, 53
Warwick, R. S., Pye, J. P., & Fabian, A. C. 1980, MNRAS, 190, 243
Wilk, M. B., & Gnanadesikan, R. 1968, Biometrika, 55, 1
Worrall, D. M., Marshall, F. F., Boldt, E. A., & Swank, J. H. 1982, ApJ, 255, 111
Wu, X.-Y., Hamilton, T. T., Helfand, D. J., & Wang, Q. 1990, Columbia Astrophysical Lab. preprint, 391

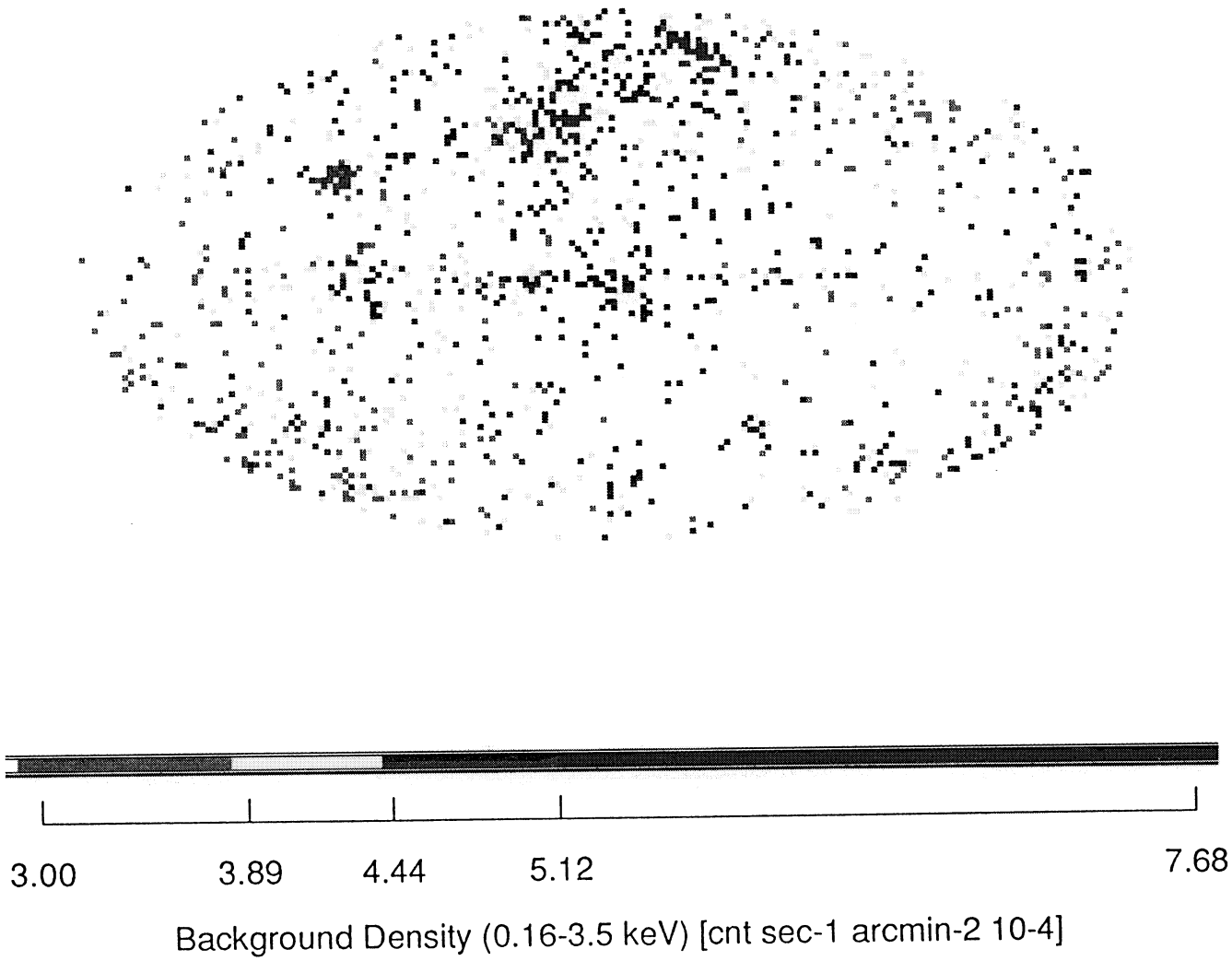

FIG. 3.—Spatial distribution of IPC fields in our sample showing the emergence of distinct spatial structure in the 0.16–3.5 keV background intensity. The false-color code—note the color-intensity scale at the lower bottom of the figure—has been chosen to show quantitatively the four intensity quartiles.

MICELA et al. (see 380, 498)

PLATE 13

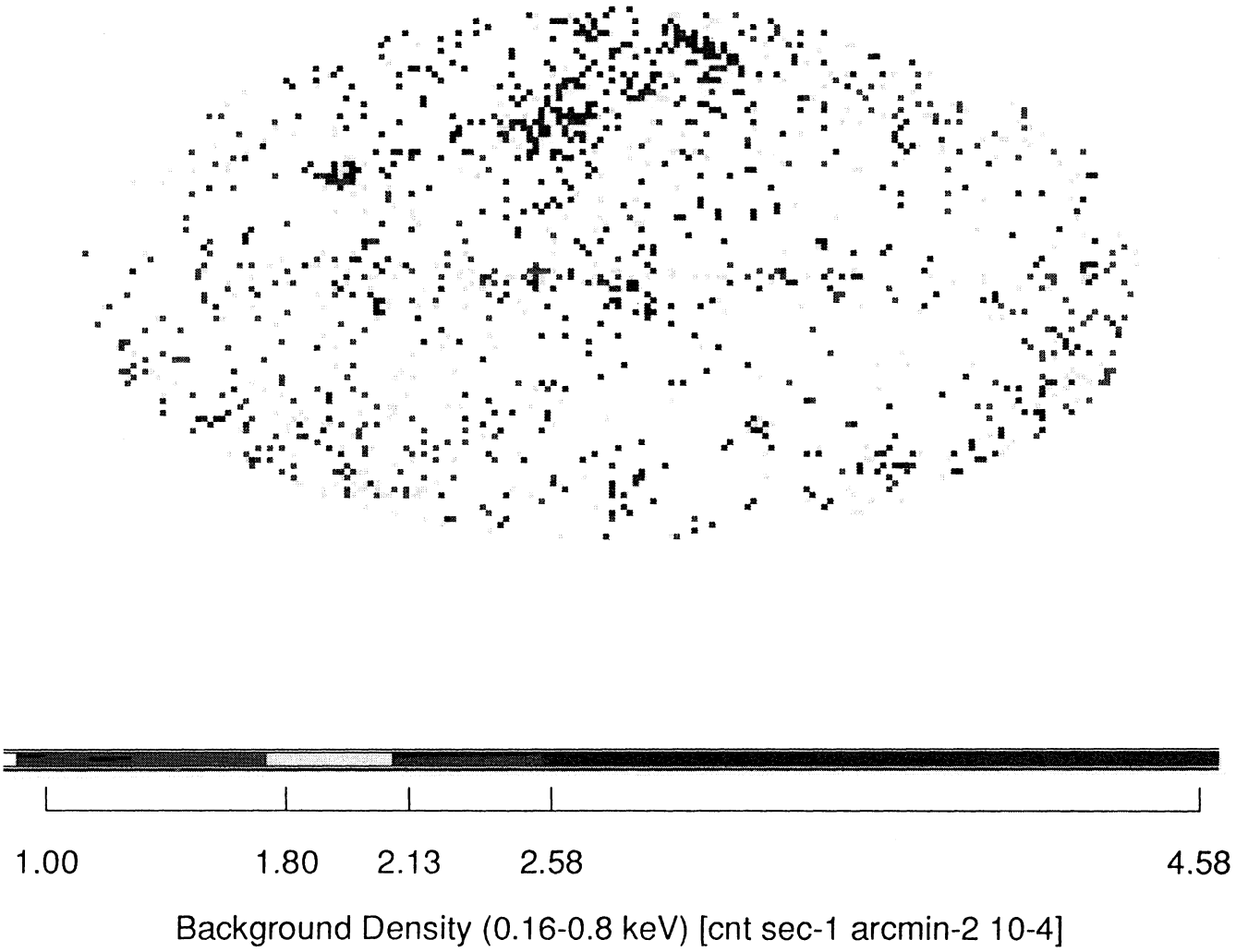

FIG. 8.—The spatial distribution of all IPC fields in this survey in the soft (0.16–0.8 keV) channels. The false-color code, indicated by the color-intensity scale at the bottom of the figure, has been chosen to show quantitatively the four intensity quartiles.

MICELA et al. (see 380, 502)

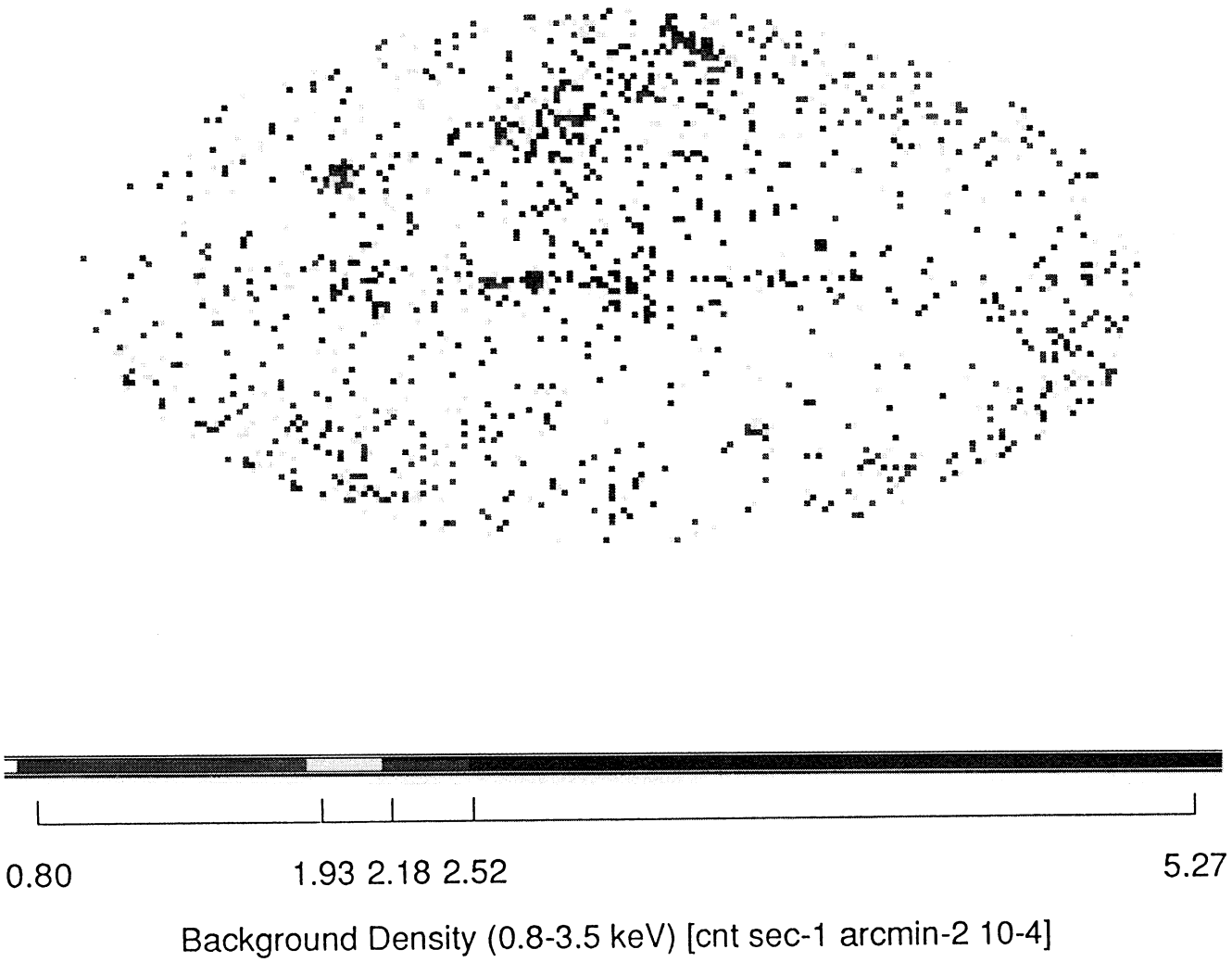

FIG. 9.—The spatial distribution of all IPC fields in this survey in the hard (0.8–3.5 keV) channels. The false-color code, indicated by the color-intensity scale at the bottom of the figure, has been chosen to show quantitatively the four intensity quartiles.

MICELA et al. (see 380, 502)

PLATE 15

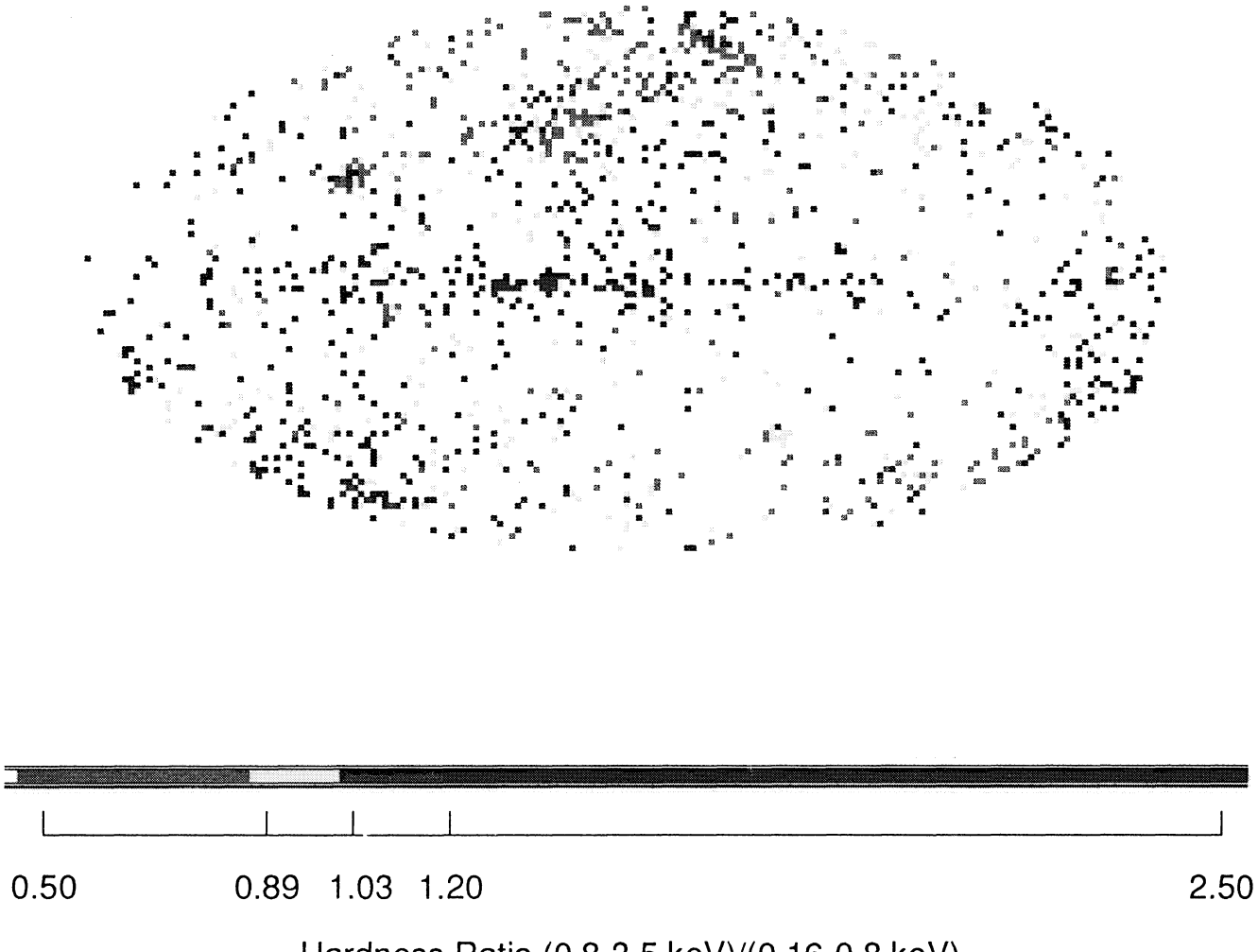

FIG. 10.—Spatial distribution of IPC fields in our sample color-coded by background hardness ratio (HR)—HR = (0.8–3.5) keV/(0.16–0.8) keV. The emergence of distinct spatial structures associated with distinct spectral trend in the background can be easily seen in this map where colors have been coded according to the four HR quartiles.

MICELA et al. (see 380, 502)